Virtual Sculpting: An Investigation of Directly Manipulated Free-Form Deformation in a Virtual Environment

THESIS

Submitted in fulfilment of the requirements

for the Degree of

MASTER OF SCIENCE

of Rhodes University

by

James Edward Gain

February 1996

Abstract

This thesis presents a Virtual Sculpting system, which addresses the problem of Free-Form Solid Modelling. The disparate elements of a Polygon-Mesh representation, a Directly Manipulated Free-Form Deformation sculpting tool, and a Virtual Environment are drawn into a cohesive whole under the mantle of a clay-sculpting metaphor. This enables a user to mould and manipulate a synthetic solid interactively as if it were composed of malleable clay. The focus of this study is on the interactivity, intuitivity and versatility of such a system. To this end, a range of improvements is investigated which significantly enhances the efficiency and correctness of Directly Manipulated Free-Form Deformation, both separately and as a seamless component of the Virtual Sculpting system.

Acknowledgements

My supervisors, Professor Dave Sewry and Professor Peter Clayton, have with their helpfulness, interest and cross-questioning made my research at Rhodes University stimulating and fruitful.

I have spent many an hour with pencil or chalk explaining my work to fellow postgraduates. My thesis has benefitted from the probing and challenging discussions that followed. The members of the RhoVeR development team have helped build the Virtual Reality system that I incorporated into this work, and for this I am extremely grateful.

My family have always provided a constant background of encouragement and bolstering, even when they did not understand why I always seemed to be playing with black Lycra gloves and visorless helmets.

Ingrid van Eck has many times rightly felt that she was writing this thesis alongside me. Without her by my side, proofreading over my shoulder, "surfing the net" while I worked, occasionally "cracking the whip" and always giving love and patient support, this thesis would have been an insurmountable task.

Thanks also are due to my proofreading "team": Shaun Bangay, Prof. Peter Clayton, Prof. Dave Sewry, Ingrid van Eck and Greg Watkins, who have dissected the mathematics and grammar of this thesis.

I acknowledge the financial support of Rhodes University and the Foundation for Research Development.

Contents

Chapter 1

Introduction

1.1 Solid Modelling

Solid Modelling is a significant subdiscipline of Computer Graphics concerned with designing three-dimensional objects on computer. The field has diverse applications, both in manufacturing, where, under the guise of Computer Aided Design (CAD), it is pervasive, and as a component in most Computer Graphics creation pipelines. For instance, it is critical to the design of cars, ships and aircraft, complex mechanical parts and architectural structures, as well as Computer Animated models and Virtual Reality scenes. These two spheres mirror the division of Solid Modelling into functional and free-form [Miller 1986]. Free-Form Modelling is concerned only with the aesthetics of the final shape. In contrast, Functional Modelling considers factors such as aerodynamics, joint angles, volume, and response to heat and stress, typically through mechanisms such as Finite Element Analysis. This is not, however, a clear separation so much as a continuum of constraint. At one pole, a computer sculptor is influenced only by his imagination and at the other, a gear train may have to satisfy a plethora of constraints. Alternatively, the design of a motor vehicle's shell, which must link engineering considerations with a nebulous sleekness, would fall somewhere in between.

Free-Form Solid Modelling is guided by three criteria:

1. **Intuitivity.** The user should be able to apply insight garnered from everyday tasks to an unfamiliar modelling environment.
2. **Interactivity.** The response-time of the system should be such that delays do not hinder creative design.
3. **Versatility.** The user should be able to convert intentions and requirements into a designed result with ease and precision.

These principles exist in constant tension. Focusing on one aspect tends to wrench the others out of balance. Enhanced versatility, for example, may increase conceptual and computational complexity to the detriment of the intuitive and interactive facets of a system. During construction, a modelling system must be measured constantly against these ideals.

1.2 Classification of Modelling Systems

Free-Form Solid Modellers can be separated into three components: Representation, Tools and Environment. These correspond loosely to data-structures, algorithms and interfaces.

1.2.1 Representation

A Representation is a means of encoding the shape of a solid object. Some modelling systems may capture properties such as colour and texture, but for free-form design, shape is sufficient. There are four principle categories of representations [Foley *et al 1991*]:

1. **Boundary Representations (B-Reps).** Here, an object is defined by its topological boundary and the internal structure is ignored. B-Reps may be either Polyhedral, where the surface is a faceted approximation composed of adjoining polygons, or Non-Polyhedral, where the surface is sewn from parametric bicubic patches. The Polygon-Mesh is an example of a Polyhedral B-Rep. At its most elementary it

consists of a list of faces, each of which is a sequence of pointers into a vertex list. In contrast, the popular Non-Uniform Rational B-Spline (NURBS) supports a Non-Polyhedral B-Rep. A NURBS patch is tersely defined by a web of control points much as an elastic sheet is distorted by weights.

2. **Cell Decomposition.** The solid is formed by "glueing" together primitive elements which are themselves solids that may vary in size, shape and orientation. For example, Spatial Occupancy Enumeration is a variant in which all the primitives are identical cubes known as Voxels (Volume Elements) in analogy to Pixels (Picture Element). These Voxels can be visualized as slotting into compartments in a three-dimensional grid.

3. **Constructive Solid Geometry (CSG).** Again a solid is built from primitives (spheres, cylinders, etc.) but instead of simple non-intersecting adjacency they are combined with Regularized Boolean Set Operations (union, intersection and difference). Typically CSG solids are stored as a tree structure, where the leaf nodes are primitives, internal nodes are set operations, and the root solid is evaluated by a depth-first walk.

4. **Binary Space Partitioning (BSP).** Here a solid is sliced out of world co-ordinate space. Each slice is created by a plane which partitions space into two domains, one within and the other outside the solid.

1.2.2 Tools

A tool metaphor is unusually appropriate when referring to methods of transforming solids. A direct comparison can be made with a craftsman's use of a range of tools in realizing a design. A solid modeller would select techniques on the basis of the solid's representation and desired shape, just as a craftsman would employ different tools depending on his materials and intentions.

Solid Modelling tools can be placed in three categories [Coquillart 1987]:

1. **Modifiers.** Modifiers are tools that perturb the shape of an existing object, either within a limited area, or across the object's entirety. Examples of the latter are the

tapering, twisting and bending tools [Barr 1984]. These are proportional applications of the affine transformations (scaling, rotation and translation). By contrast, free-form surface moulding falls in the former category and is a staple of Solid Modelling. At its most primitive it involves displacing individual vertices and at its most advanced it allows complex widespread deformations.

2. **Combiners.** These methods create a synthesis of objects. Foremost among them are the Regularized Boolean Set Operations: Union, Intersection and Difference. These are three-dimensional analogues of the familiar two-dimensional set operations, extended so as to encompass solids. Regularized Boolean Set Operations are supported across the spectrum of Solid Modellers and their use is even mandated by representations such as Constructive Solid Geometry.

3. **Constructors.** Unlike the other classes of tools that modify previously developed objects, constructors build solids from nothing. At its most painstaking this entails entering vertex co-ordinates directly and expecting the computer to interpolate these values in creating a solid. Fortunately, there are less excruciating constructors such as primitive instancing, sweeping and lofting. Primitive instancing allows the selection of one of a family of parametrised three-dimensional primitives. A sweep object is constructed by sliding a two-dimensional contour along a curved path, with a goblet or wine glass being a typical result. Lofting forms objects by interpolating a series of cross-sections and is often applied to the definition of hulls, fuselages and car-bodies.

1.2.3 Environment

There is a strong symbiotic relationship between Solid Modelling and Human Computer Interaction, with each discipline feeding off innovations in the other. This is probably because the design of three-dimensional shapes is an inherently difficult task [Requicha and Rossignac 1992] which involves the user directly. Thus, design environments vary as widely as their application domains, and the range in IO devices and interaction styles is bewildering. Fortunately, modelling systems can be separated at a fundamental level into two classes:

1. **Two-Dimensional.** Interaction is funnelled through two-dimensional media. A typical interface would accept input from a mouse or light-pen and output a set of orthogonal views.

2. **Three-Dimensional.** The environment is controlled by and responds with three-dimensional mechanisms. Such systems are generally driven by six-degree-of-freedom devices and display stereoscopic images.

Some environments span this division with a hybrid of two and three-dimensional techniques.

1.3 Polygon-Mesh Representation

The Polygon-Mesh is the most elementary, stripped-down representation capable of unambiguously encoding a solid. It is an evaluated hierarchical structure of faces, edges and vertices, which often serves as a link between the domains of modelling and rendering. Typically, more sophisticated unevaluated representations are reduced to a Polygon-Mesh before being piped to the rendering engine. The weaknesses of the Polygon-Mesh stem from approximation. It breaks curved surfaces into planar subdivisions (polygonal facets) that only hint at the intended curves. This is disastrous when accuracy is a prerequisite and tolerances are hair-fine, as in many functional applications. However, Free-Form Modelling does not enforce such rigour and benefits considerably from the speed and simplicity of the Polygon-Mesh.

1.4 Sculpting Tools

There is a class of Free-Form Modifiers whose premise is the deformation of solids in a physically realistic fashion. They loosely simulate carving or moulding inelastic substances, such as modelling clay, Plasticine and silicone putty.

There is considerable research into adapting Finite Element Theory to this task. In essence

the Finite Element Method subdivides a solid or its boundary into small regular elements, imposes a set of forces such as gravity, inertia, internal stress and external pressure, and then calculates an equilibrium of shape among the volume elements. This approach is highly realistic, since it directly incorporates mechanics, but it is space and computation intensive. For instance, the interaction of a hand and ball in a grasping task has been modelled [Gourret *et al* 1989] down to the level of muscle, skin and bone flexion and deformation, but only in a Computer Animation context where individual frames may take hours to process. Also, a variety of precise deformation phenomena have been developed [Terzopoulos and Fleischer 1988], namely Viscoelasticity (where shape is fluid under sustained pressure but reacts like solid rubber to transient force), Plasticity (where the solid deforms irrevocably under pressure) and Fracture (which simulates tearing and shredding in brittle substances). Again, this is utilized in Computer Animation although the authors claim that "it should be possible to animate such inelastic dynamics in real-time in three dimensions on a supercomputer" [Terzopoulos and Fleischer 1988]. Since then the use of Finite Elements has been honed through a range of restrictions. The ShapeWright [Celniker and Gossard 1991] paradigm restricts interactive deformation to toggling surface parameters such as bending resistance and internal pressure. Here design is in three stages: first the shape's character lines are traced as curve segments, then the solid's "skin" is stretched between these curves, and finally surface parameters are adjusted. An alternative approach is to limit the choice of initial shapes to simple primitives (spheres, ellipsoids, etc.) while allowing sophisticated deformation [Metaxas and Terzopoulos 1992]. The pinnacle of this trend is the merging of a Triangular B-Spline Patch Representation with physically based Finite Element Methods [Qin and Terzopoulos 1995].

At the other end of the complexity spectrum are the proportional affine transformations [Barr 1984] and Decay Functions [Bill and Lodha 1994]. The former mimics tapering by scaling proportionally along an axis, twisting by progressive rotation along an axis and bending by a combination of rotation and translation. The latter propagates the translation of a vertex to its surrounding region according to a bell, cusp or cone-shaped template. Both tools are extremely efficient but of limited utility. For example, Decay functions do not cater for the complex interaction of a multiplicity of translated vertices and proportional affine transformations offer only specific stylized alterations.

Between these extremes are the constraint-based tools of Variational Solid Modelling

[Welch and Witkins 1992] and Directly Manipulated Free-Form Deformation
[Hsu *et al* 1992, Borrel and Bechmann 1992] that meld efficiency and versatility. Variational Surfaces are infinitely malleable and have no fixed controls. They are defined by a collection of constraining points and curves, much as an elastic sheet would be stretched over a bed of spikes. Later topology enhancements [Welch and Witkins 1994] snap, slice and smooth these sheets together to form complex solids. Directly Manipulated Free-Form Deformation (DMFFD) is less constructive and more modifying, and is based on an ambient space-warp controlled by dragging points on the solid's surface. Both techniques are independent of representation, but in a subtly different sense. Variational surfaces are underlying and can be realized in any representation, while DMFFD is overlaying and can be applied to any representation. At their core, both rely on Linearly Constrained Optimization, a numerical scheme for optimizing an objective function (in this case a "fitness" metric such as continuity) while obeying a set of linear constraints (the directly manipulated points and curves). DMFFD has an edge in efficiency since it optimizes a sum of squares while Variational Surfaces are forced to optimize a more general quadratic function.

1.5 Virtual Environments

Virtual Reality is a protean field with almost as many definitions as their are proponents. These range from the pragmatic to the esoteric, but all include the key elements of **interaction** (the user and environment respond to each other in real-time) and **immersion** (the user has the illusion of being inside the environment) [Rheingold 1991]. A good working definition in this regard is:
"A human-computer interface where the computer and its devices create a sensory environment that is dynamically controlled by the actions of the individual so that the environment appears real to the participant." [Latta 1991]
In some circles Virtual Reality is regarded as a critical failure. This perception is due to a handful of factors. Current environments are plagued by high **latency** (a jarring delay between the user initiating an action and the system responding) and low **resolution** (a grainy block-like display of the Virtual Environment). The title of the field itself has contributed to overblown expectations, with the result that researchers now employ less ambitious terminology, such as Virtual Environments and Augmented Reality. Despite

this pessimism, the fledgling discipline is viewed by many [Requicha and Rossignac 1992, Nielson 1993, Jacobson 1994] as an ideal interface for Solid Modelling due to its intrinsically three-dimensional and interactive nature. Virtual Reality is sometimes described as "a solution in search of a problem" and one researcher [Requicha and Rossignac 1992] goes so far as to attribute to Solid Modelling the rôle of the driving "problem".

There has been some nascent research in this area. Galyean's Sculpting System [Galyean and Hughes 1991] utilizes a Voxmap data-structure (in analogy to Bitmap) to store a Cell Decomposition representation. A range of tools such as a "toothpaste tube", which trails Voxels across the solid's surface, a "heat gun", which deletes Voxels and "sandpaper", which averages Voxels across the surface, are implemented and controlled with a Polhemus Isotrak device, which locates the position and orientation of a sensor.

3-Draw [Sachs *et al* 1991] constructs skeletal objects by tracing curves and cross-sections in three dimensions with two Polhemus trackers; one fastened to a pen, with which the wireframe is sketched, and the other to a stylus, which serves as a frame of reference.

3DM (Three-Dimensional Modeller) [Butterworth *et al* 1992] borrows from the success of two-dimensional drawing programs. The user selects from a virtual toolbox with extrusion, sweeping, primitive instancing, cutting, pasting, and copying functions. The system employs a VPL Eyephone head-mounted display for **stereoscopic** viewing, a Polhemus tracker mounted on head and hand, and a proprietary Pixel-Plane graphics rendering engine.

MOVE (Modelling Objects in a Virtual Environment) [Brijs *et al* 1993] focuses on improving depth perception (with devices such as virtual walls and workbenches) and feedback (through sight, sound and tactile cues) in simple design tasks, such as scaling, connecting and separating objects, and moving vertices.

DesignSpace [Chapin *et al* 1994] is an ongoing project intended to support mechanical design. The project has proceeded on two primary fronts: dextrous manipulation, where hand-eye co-ordination in Virtual Reality is enhanced, and remote collaboration, where several people participate simultaneously and interactively in a design.

THRED (Two Handed Refining Editor) [Shaw and Green 1994] incorporates both hands, each tracked by a Polhemus sensor, into the process of modelling polygonal surfaces. The

dominant hand selects and manipulates vertices, while the less dominant hand sets such contexts as the position and orientation of the scene and level of subdivision of the surface.

These exploratory forays do not (with the exception of DesignSpace) exploit the true potential of Virtual Reality in Solid Modelling, since deformation is either specified by a single three-dimensional point (THRED, 3DM, 3-Draw, Galyean Sculpting) or limited glove input (MOVE), and in most cases (THRED, MOVE, 3DM, 3-Draw), only rudimentary modifiers are implemented.

1.6 Focus of Research

This project imposes a clay-sculpting metaphor on the Free-Form Solid Modelling process. The intention is to link the familiar physical action of moulding clay to the unfamiliar task of computerised shape design. The underlying concern in this project is the balance and enhancement of the triad of Free-Form Modelling principles: interactivity, intuitivity and versatility.

Three pivotal design decisions were made early in this research. The Polygon-Mesh, with its uncluttered simplicity and efficiency, was chosen as a representation. Directly Manipulated Free-Form Deformation was selected as a sculpting tool, because it is intuitive in its fluid, graceful deformations, versatile in its scope of application, and comparatively interactive. A Virtual Environment was picked as the interface because the elements of interaction and immersion contribute a "hands-on" immediacy, and thus intuitivity, to modelling.

The Free-Form Solid Modelling system developed in this thesis can now be characterized. It binds a Polygon-Mesh representation, Directly Manipulated Free-From Deformation tools and a Virtual Environment within the cohesive framework of a clay-sculpting metaphor. This thesis focuses on the interactivity, intuitivity and versatility of such a system.

1.7 Thesis Organisation

The remainder of this thesis is structured as follows:

- **Chapter 2 (Foundations)** presents the basics of Directly Manipulated Free-Form Deformation and considers the innate strengths and weaknesses of the three tiers, Splines, Free-Form Deformation and Direct Manipulation, that make up the technique.
- **Chapter 3 (Least Squares Solution Methods)** focuses on the efficiency of DMFFD. The core computation, a linearly constrained least squares optimization, is examined, and a new, considerably less space- and computation-intensive algorithm is developed.
- **Chapter 4 (Topology and Correctness Issues)** focuses on the correctness of DMFFD. The situations in which DMFFD creates invalid self-intersecting solids are discussed. Methods of refining and decimating the Polygon-Mesh in order to maintain a smooth sculpted appearance are also considered.
- **Chapter 5 (Applications)** describes the RhoVeR (Rhodes Virtual Reality) system which forms a testbed for Virtual Sculpting. Two illustrative applications, glove-based moulding and dynamic surface sketching, are developed.
- **Chapter 6 (Conclusion)** presents concluding remarks and suggests directions for future research.
- **Appendix A (Colour Plates)** displays the Virtual Reality equipment and illustrates Glove-based Moulding.
- **Appendix B (Directly Manipulated Free-Form Deformation Program Extracts)** lists pivotal sections of the Virtual Sculpting system code.
- **Appendix C (Specification of the RhoVeR System)** provides design and implementation details of the Rhodes Virtual Reality System.

Chapter 2

Foundations

Free-Form Deformation, when coupled with Direct Manipulation, is a powerful and versatile approach to Solid Modelling. The technique allows the displacement of one or more points on a solid, with the surface surrounding these points conforming as if the solid were composed of malleable clay. Directly Manipulated Free-Form Deformation (DMFFD) provides intuitive control and predictable, aesthetic results but is burdened by notorious inefficiency. DMFFD relies on an intricate body of theory, built in three tiers: Splines, Free-Form Deformation and Direct Manipulation. This chapter is devoted to an exploration of this theory. The mathematics, data structures, algorithms and, most importantly, efficiency concerns are examined at each level.

2.1 Splines

At the turn of the century the term **spline** was widespread only in ship design. It meant a strip of flexible metal which had been contoured with weights to fit the shape of a boat's keel. Appropriately, when ship design was computerised, so too was the spline.

In its modern usage a spline is the basis for a curve that is regulated by a series of control vertices. Splines fall into two categories: **Interpolating**, where the curve passes through the control vertices and **Approximating**, where the vertices guide and channel the curve.

A spline-based curve is a piecewise polynomial that is composited of segments joined smoothly end to end. Each of these segments is a weighted sum of control vertices with the weights determined by a spline-function.

This description will be clarified by the development of the **Uniform Rational Basis-Spline**, a family of approximating splines with many useful properties [Bartels *et al 1987*].

2.1.1 Uniform Rational Basis-Splines

2.1.1.1 Linear (First Order)

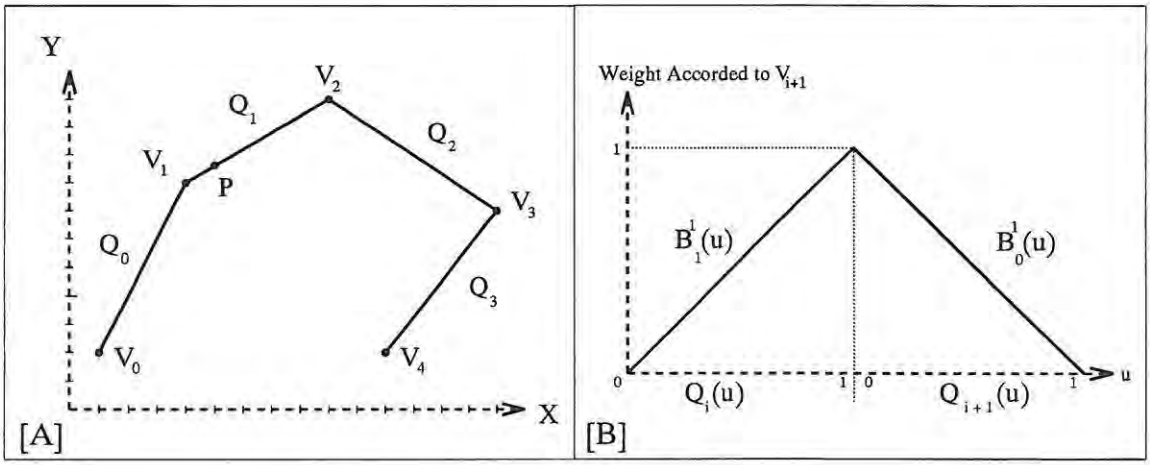

Figure 2.1: The Uniform Linear B-Spline. [A] An example curve. [B] The basis-functions.

A simple polygonal arc (a sequence of straight line-segments) can be considered a rudimentary spline and will provide a foundation for higher-order generalizations. A line-segment (Q_i) can be parametrised with a control variable (u) so as to interpolate its endpoints (V_i and V_{i+1}) as:

$$Q_i(u) = u \cdot V_{i+1} + (1-u) \cdot V_i \qquad u \in [0,1] \tag{2.1}$$

For instance, $P = Q_1(0.2) = 0.8 \cdot V_1 + 0.2 \cdot V_2 = (5, 8.6)$ in figure 2.1. Now Equation 2.1 can be recast in summation notation.

$$
\begin{aligned}
Q_i(u) &= \sum_{r=0}^{1} B_r^1(u) \cdot V_{i+r} \qquad u \in [0,1] \qquad (2.2)\\
B_0^1(u) &= (1-u)\\
B_1^1(u) &= u
\end{aligned}
$$

B_0^1 and B_1^1 are the basis functions of the Uniform Linear B-Spline. The terminology of the previous section can now be clarified. Each segment ($Q_i(u)$) is a sum of control vertices (V_i and V_{i+1}) weighted by a spline basis (B_0^1 and B_1^1). The linearity of this spline manifests itself in two ways: The bases are first-order (linear) polynomials in u and consequently each segment (Q_i) is a linear function of u.

2.1.1.2 Quadratic (Second Order)

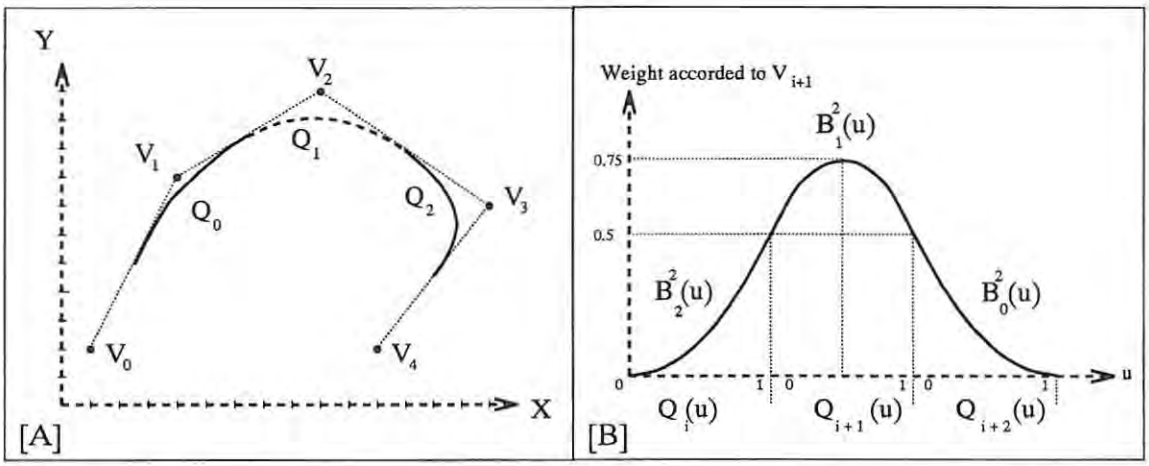

Figure 2.2: The Uniform Quadratic B-Spline. [A] An example curve. [B] The basis-functions.

Stepping up from linear to quadratic splines makes each segment dependent on an extra vertex (notice the increase in the index of summation from equation 2.2 to 2.3).

$$
\begin{aligned}
Q_i(u) &= \sum_{r=0}^{2} B_r^2(u) \cdot V_{i+r} \qquad u \in [0,1] \qquad (2.3)\\
B_0^2(u) &= \tfrac{1}{2} - u + \tfrac{1}{2}u^2\\
B_1^2(u) &= \tfrac{1}{2} + u - u^2\\
B_2^2(u) &= \tfrac{1}{2}u^2
\end{aligned}
$$

Each segment now traces a non-interpolating quadratic curve (as is clear from figure 2.2), since the basis-functions (B_0^2, B_1^2, B_2^2) are second-order polynomials. The same number of control vertices now define fewer segments, but each segment is smoother and more refined. The polygonal arc joining the control vertices (V_0 to V_4) is termed a **control polygon** and a segment is contained on or within the control polygon of its contributing vertices. Linear B-Splines, for instance, coincide with their control polygon.

2.1.1.3 Cubic (Third Order)

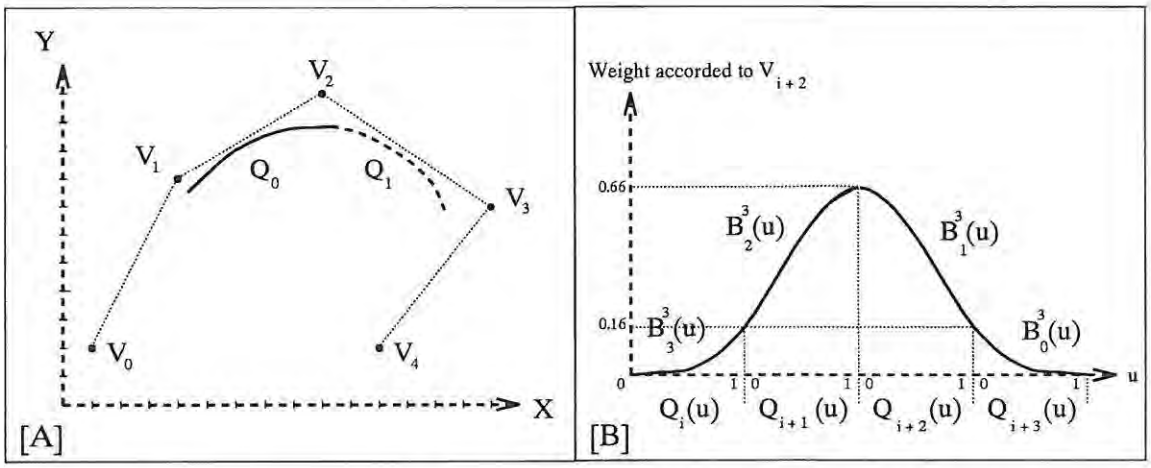

Figure 2.3: The Uniform Cubic B-Spline. [A] An example curve. [B] The basis-functions.

The generalization can be further extended to cubic splines, which produce even more tapered effects.

$$
\begin{aligned}
Q_i(u) &= \sum_{r=0}^{3} B_r^3(u) \cdot V_{i+r} \qquad u \in [0,1] \qquad (2.4)\\
B_0^3(u) &= \tfrac{1}{6}(1 - 3u + 3u^2 - u^3)\\
B_1^3(u) &= \tfrac{1}{6}(4 - 6u^2 + 3u^3)\\
B_2^3(u) &= \tfrac{1}{6}(1 + 3u + 3u^2 - 3u^3)\\
B_3^3(u) &= \tfrac{1}{6}u^3
\end{aligned}
$$

The pattern continues as each segment is influenced by 4 ($order + 1$) control vertices ($V_i, V_{i+1}, V_{i+2}, V_{i+3}$), each of which is scaled by a cubic basis-function ($B_0^3, B_1^3, B_2^3, B_3^3$).

2.1.1.4 Properties

With this background in place, the pivotal properties of Uniform B-Splines can be examined.

- **Continuity.** A piecewise curve is considered to be of C^n continuity if at every point along the curve the n^{th} derivative exists and is continuous. In particular, this condition must hold at the joints between segments. This provides a useful measure of curve continuity. The basis-functions of figures 2.1, 2.2 and 2.3 track the influence of a single control vertex across neighbouring segments. The continuity of the basis-functions and the curves born of them are identical because each curve segment is merely a linear combination of scaled basis-functions (as is evident from equations 2.2 - 2.4). The basis-functions of figure 2.1 exhibit only C^0 or positional continuity, which explains the jagged appearance of their corresponding curves. In contrast, quadratic and cubic B-splines produce C^1 and C^2 continuity respectively.

- **Local Control.** Each segment of a curve is determined by a fixed subset (cardinality $order + 1$) of control vertices. Conversely, a single control vertex affects only a portion ($order + 1$ segments) of the curve. Thus B-Splines allow detailed design of subsections of a curve.

- **Convex Hull.** Every segment lies entirely within its control polygon, and the entire curve is confined within the convex hull of all control vertices. A convex hull can be visualized as an elastic band snapped around the outside of the vertices. These properties impart a useful degree of predictability to Uniform B-Splines.

- **Efficiency.** The inherent simplicity of the Uniform B-Spline family enhances their speed above that of more convoluted splines. There are two key factors in this: (a) the uniformity of the parametrisation of u which spans a set $[0, 1]$ interval and (b) the dedication of all free variables ($order + 1$ coefficients of each basis-function) to attaining $C^{order-1}$ continuity and none to extraneous concerns such as interpolation. Evaluating the basis-functions for a given parameter value u becomes progressively more costly from linear (1 addition) to cubic B-Splines (10 multiplications and 8 additions).

2.1.2 Other Splines

Splines are a field of intense interest and frenetic research. There are many extensions to Uniform B-Splines, for instance Non-Uniform Rational B-Splines (NURBS) [Foley *et al 1991*], which relax the uniform unit interval restriction and are much in vogue, as well as β-Splines [Bartels *et al 1987*], which introduce bias and tension parameters. Their collective purpose is to allow finer control over the curve and increase the diversity of shape and continuity. However, these enhancements are unnecessary in this context because splines are hidden from the user under several layers of indirection. The enhanced splines invariably introduce extra parameters, which would damage the illusion of sculpting because their effects are often neither intuitive nor obvious. Further, this added complexity always carries a baggage of extra calculation.

2.2 Free-Form Deformation

Free-Form Deformation (FFD) employs an unusual approach to Solid Modelling. It warps the space surrounding an object and thereby transforms the object indirectly. An analogy would be setting a shape inside a square of jelly and then flexing this jelly, resulting in a corresponding distortion in the embedded shape.

This is achieved by imposing a lattice of control vertices on a portion of world co-ordinate space. These can be pictured as hooks plunged into the jelly, which are used to distort its shape. Any point in this demarcated space becomes a weighted sum of these lattice control vertices.

The lattice is a direct extension of the splines introduced in the previous section. While splines can be anchored in a space of any dimension, they remain strictly one-dimensional. It is helpful to picture an infinitely thin ribbon twisting and contorting through the air. This dichotomy arises from the different dimensions of the control vertices (V_i), which are points in the world co-ordinate space of the modelling application (generally two or three-dimensional), and the basis-functions, which are reliant on a single parameter u and are thus one-dimensional. FFD extends spline-curves to two-dimensional areas and three-

dimensional volumes, so that the dimensions of the spline and its control vertices match. At each step up in dimension an extra parameter is introduced, v for areas and then w for volumes, and the control polygon becomes first a control grid, then a control lattice. Under this generalization a spline volume is traced out by:

$$Q_{i,j,k}(u,v,w) = \sum_{r=0}^{\alpha}\sum_{s=0}^{\alpha}\sum_{t=0}^{\alpha} B_r^{\alpha}(u)\cdot B_s^{\alpha}(v)\cdot B_t^{\alpha}(w)\cdot V_{i+r,j+s,k+t} \qquad (2.5)$$

$$u,v,w \in [0,1]$$

α = the order of the spline
V = a vertex in the control lattice
B^{α} = the basis functions, B^0 = linear, B^1 = quadratic, B^2 = cubic
u,v,w = control variables
Q = a point in the spline volume

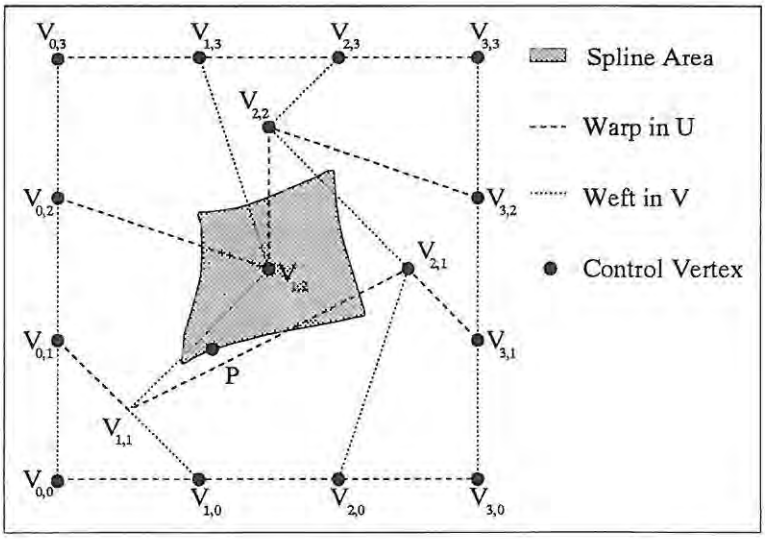

Figure 2.4: Two-dimensional Cubic B-Spline Area defined by a Control Grid.

It is instructive to compare this with the curves of the previous section (equations 2.2 - 2.4). Here the position of points trapped in the spline volume are dictated by $(\alpha+1)^3$ control vertices instead of a mere $(\alpha+1)$ and each control vertex is scaled by three basis-functions rather than one.

Equation 2.5 is manifested in the distorted patch of figure 2.4. This is a two-dimensional

area based on a cubic B-spline, so that the w parameter is dispensed with and the area is determined by 16 (4×4) control vertices. **For Example:** $P(0.2, 0.0) = (1.143, 0.938)$ with $V_{0,0} = (0.0, 0.0)$ and $V_{3,3} = (3.0, 3.0)$ in world co-ordinates.

The piecewise nature of spline-curves is maintained so that areas and volumes can be stitched together. In the case of spline areas, adding $(\alpha + 1)$ control vertices in either direction enlarges the surface by a cell in that direction. Spline volumes require a slice of $(\alpha + 1) \times (\alpha + 1)$ vertices to create adjoining cells.

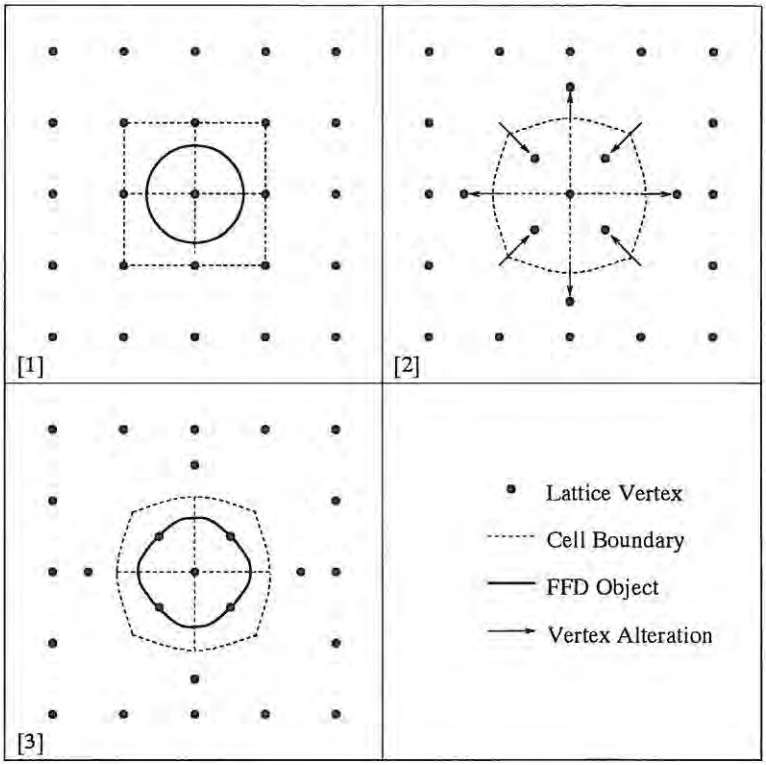

Figure 2.5: The Three Stages of FFD. [1] Embedding the Object, [2] Moving Lattice Vertices, [3] Deforming the Object.

Now, the Free-Form Deformation process can be unfolded into three stages (as shown in figure 2.5):

1. An undistorted or base-state lattice is generated. It has vertices spaced regularly in **orthogonal** u, v, w directions. This demarcates a number of box-shaped (or **parallelpiped**) spline volumes, hereafter referred to as cells. This is analogous to taking a cube of jelly fresh from its mould. Then the surface points of the

designed object are parametrised within this lattice. They are located within a cell (referenced by the i, j, k index of its corner lattice vertex) and given local u, v, w co-ordinates relative to the cell origin $(0.0, 0.0, 0.0)$ and maximum extent $(1.0, 1.0, 1.0)$. If equation 2.5 is applied to a given parametrisation at this stage, the original point is recaptured. In terms of the metaphor, the shape being squished is set inside the jelly.

2. A number of lattice vertices are displaced, with a consequent distortion of lattice cells. This equates to flexing the jelly by wrenching on the embedded hooks.

3. The parametrised surface points (i, j, k and u, v, w) are churned through equation 2.5 to spawn an altered shape, whose deformation mirrors that of the cells in which it lies. So, by the analogy, the inset shape is warped along with its cocooning jelly.

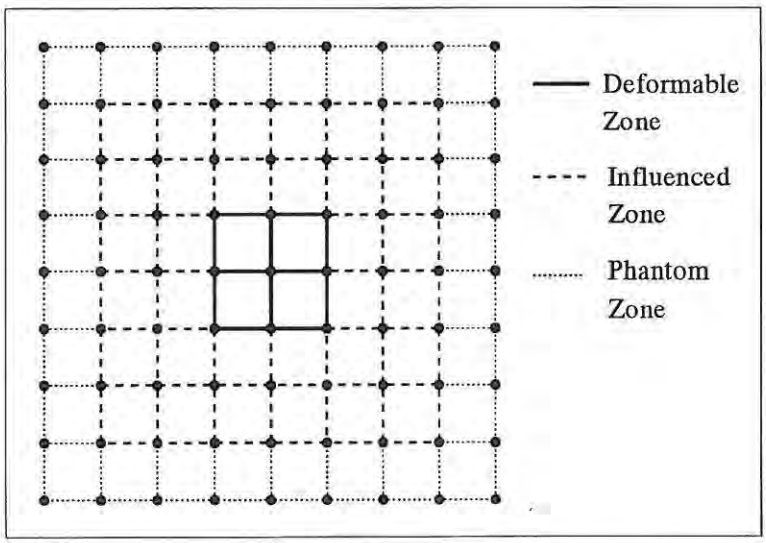

Figure 2.6: A FFD lattice showing Deformable, Influenced and Phantom Zones.

The fringes of the lattice may, without careful attention, produce anomalous continuity degradation. To prevent this, the lattice is partitioned into three rings. At the centre is the deformable zone, with any number of vertices and their corresponding cells. Around this lies the influenced zone of cells affected by the movement of control vertices in the deformable zone. At the edges a phantom zone of static vertices guards against boundary conditions. These phantom vertices are preferred to the tripling up of vertices previously proposed [Hsu *et al* 1992], since this introduces additional complexity into the FFD algorithm.

Figure 2.7: Free-Form Deformation

Purpose: Displace object points with Free-From Deformation.
Given: V A 3D lattice of control vertices,
P A list of object points,
m The number of entries in P.
Return: An FFD-altered version of P.
Data Structures: (i, j, k) Indices of a lattice cell,
(u, v, w) Co-ordinates within a lattice cell.

```
FOR α = 1, 2, ..., m
    IF P_α lies within the influenced or deformable zones
    of the lattice THEN
        parametrise P_α with (i, j, k) indices
        and (u, v, w) co-ordinates
        P_α ⟵ (0.0, 0.0, 0.0)
        FOR r = 0, ..., 3
            FOR s = 0, ..., 3
                FOR t = 0, ..., 3
                    P_α ⟵ P_α + V_{i+r,j+s,k+t} × B_r^3(u) × B_s^3(v) × B_t^3(w)
```

A two-dimensional analogue of a multi-cell cubic B-spline lattice is detailed in figure 2.6, and the FFD algorithm associated with this data structure is outlined in figure 2.7.

This highlights the inherent inefficiency of FFD. Every point of an object within the scope of the lattice (potentially hundreds) undergoes 64 iterations involving 3 multiplications and an addition. The basis-functions can be calculated outside the inner loop, but their calculation, as well as the parametrisation of surface points, still adds significantly to this inefficiency.

There are, however, several means of improving matters:

- In the original FFD [Sederberg and Parry 1986] and later extensions, the lattice is allowed arbitrary orientation relative to the world co-ordinate (x, y and z) axes. This does not increase the range of possible deformations and it substantially complicates the evaluation of local co-ordinates. Instead, the (u, v, w) axes of the lattice are oriented so that they lie parallel to the (x, y, z) axes.

- There may be cells whose control vertices are unaltered and which do not perturb points falling within them. Instead of executing the body of the FFD loop only to return the original point unchanged, a Boolean index, which flags cells with altered

vertices, can be consulted. In this way, if a lattice control vertex is moved, then the 64 cells influenced by this vertex are marked in the index.

- The Uniform Cubic B-Splines are the most efficient of all the splines with comparable smoothness. However, if the user is willing to accept less tapered results, then the Uniform Quadratic B-Splines of equation 2.3 can be substituted to good effect. Now the inner loop has 27 ($3 \times 3 \times 3$) iterations and the calculation of the basis-functions is almost twice as fast. Technically, this is downgrading from continuity of second derivatives (class C^2) in the case of the Cubic B-Spline, to continuity of first derivatives (class C^1) for the Quadratic B-Spline.

The Free-Form Deformation technique was first presented in a seminal paper [Sederberg and Parry 1986], which has sparked widespread academic research and commercial application. There are three primary avenues along which FFD has developed:

- **Animation.** FFD has cross-pollinated well with the discipline of Computer Animation. *Layered Construction for Deformable Animated Characters* [Chadwick *et al* 1989] builds animated figures from their articulated skeletons outwards and FFD is utilized to simulate the flex and ripple of the muscle and tissue layers. *Animated Free-Form Deformation* [Coquillart and Jancène 1991] gradually translates objects through a distorted lattice to induce dynamic deformations. For instance, a tube can be made to bulge and swell progressively down its length.

- **Generalisation.** There were two aspects of the original FFD [Sederberg and Parry 1986] which invited generalisation: the base-state lattice with its structure of vertices regularly spaced in a parallelpiped arrangement, and the Bezier curve underpinnings. *NURBS-Based Free-Form Deformations* [Lamousin and Waggenspack 1994] substitutes Non-Uniform Rational B-Splines in place of Bezier curves and thus allows vertices to be unevenly spaced along the orthogonal axes of the initial lattice. *Extended Free-Form Deformation* [Coquillart 1990] introduces complex configurations for base-state lattices, which fit more snugly around the object being shaped and thereby establish greater control and predictability.

- **Direct Manipulation.** *Deformation of N-Dimensional Objects* [Borrel and Bechmann 1992] provides a method for controlling the surface of an

embedded solid directly. The same results were independently and more narrowly formulated in *Direct Manipulation of Free-Form Deformation* [Hsu *et al* 1992]. It is this last avenue which is explored in the next section.

2.3 Direct Manipulation

Controlling deformations by moving lattice vertices, while producing sculpted results, tends to be cumbersome and counter-intuitive. Specifying even simple deformations requires a good working knowledge of Splines and FFD. Also, the display of the lattice tends to clutter the screen and obscure the object being created. It would be preferable for the user to drag object points directly and have the surrounding points conform as if the object were malleable clay. This is the intention behind the Direct Manipulation (DM) extensions to FFD [Hsu *et al* 1992, Borrel and Bechmann 1992]. For instance, pushing or pulling a single object point will create dimples or mounds in the object's surface. More complex manipulation can be achieved by simultaneously moving several points and calculating the lattice changes required to induce these effects. The general principle behind DMFFD is first to reverse-engineer alterations in the lattice vertices, and then apply this new lattice to the original object.

To achieve this some mathematical foundations must first be layed. The algorithm of figure 2.7 can be concisely expressed in matrix form:

$$AX = B$$

where $\boxed{B}$ is an $m \times 3$ matrix formed directly from the list P,
with each row capturing the (x, y, z) co-ordinates of an object point.

$\boxed{X}$ is an $n \times 3$ matrix of the co-ordinates of all the lattice vertices $(V_{i,j,k})$ that affect the points in B. It can be formed by cycling through points in P and placing in X, without duplication, all vertices that influence a point.

$\boxed{A}$ is an $m \times n$ matrix of blended basis functions with the weight entry in column i of A matched to its vertex in row i of X. A particular (i, j) entry of A is zeroed if the vertex in row j of X does not affect the point in row i of B.

EXAMPLE

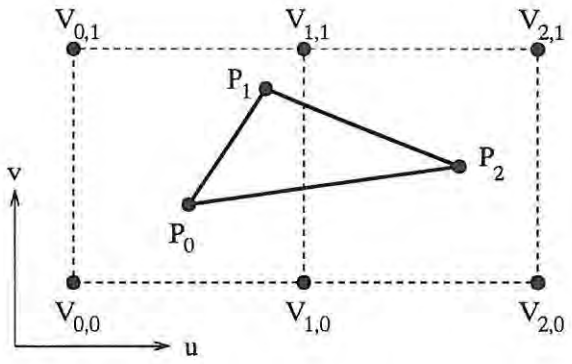

The above diagram shows a two-dimensional base-state linear lattice with a triangle inset. The triangle has points P_0, P_1, P_2 with parametrisations of $(u_0, v_0), (u_1, v_1), (u_2, v_2)$. The equation below is in essence a recasting of equation 2.5.

$$\begin{bmatrix} B_{0,0}(u_0,v_0) & B_{1,0}(u_0,v_0) & 0 & B_{0,1}(u_0,v_0) & B_{1,1}(u_0,v_0) & 0 \\ B_{0,0}(u_1,v_1) & B_{1,0}(u_1,v_1) & 0 & B_{0,1}(u_1,v_1) & B_{1,1}(u_1,v_1) & 0 \\ 0 & B_{0,0}(u_2,v_2) & B_{1,0}(u_2,v_2) & 0 & B_{0,1}(u_2,v_2) & B_{1,1}(u_2,v_2) \end{bmatrix} \begin{bmatrix} V_{0,0} \\ V_{1,0} \\ V_{2,0} \\ V_{0,1} \\ V_{1,1} \\ V_{2,1} \end{bmatrix} = \begin{bmatrix} P_0 \\ P_1 \\ P_2 \end{bmatrix}$$

$$B_{i,j}(u,v) = B_i^1(u) \times B_j^1(v)$$

Normally FFD evaluates the altered positions of object points (B) by multiplying the basis matrix of spline weights (A) and the list of control vertices (X), but Direct Manipulation reverses this. The user specifies a selection of object points and their intended motion (B), and the alteration in vertices (X) is found. In mathematical terms we seek to find X in the equation $AX = B$, given A and B. Figure 2.8 unfolds Direct Manipulation in three steps:

1. **Setup** A base-state lattice is established, the object is embedded and the user defines a number of Direct Manipulation vectors of the form "move this object point from here to there". In concrete terms matrices A and B are created. The algorithm for this step is presented below in Figure 2.9.

2. **Lattice Vertex Determination** The alterations in Lattice Vertices necessary to satisfy the DM vectors are reverse-engineered. This is an extremely involved task which consumes by far the bulk of computation, and it is the focus of the next chapter.

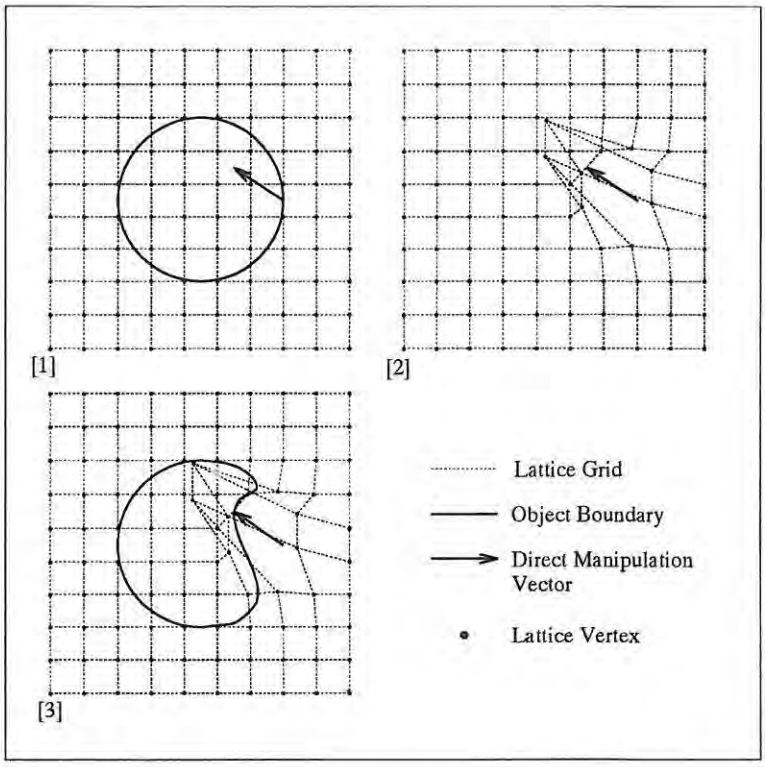

Figure 2.8: Three Stage Direct Manipulation. [1] Setup, [2] Lattice Vertex Determination, [3] Object Transformation.

3. **Object Transformation** The entire object undergoes FFD (as per the algorithm of Figure 2.7). Notice from figure 2.8 how the twin demands of matching DM vectors and a smooth clay-like deformation are satisfied.

Figure 2.9: Direct Manipulation Setup

Purpose:	Prepare the Mathematical Foundations of Direct Manipulation.	
Given:	V	A 3D FFD lattice,
	D	A set of Directly Manipulated object points,
	ΔD	A set of Direct Manipulation vectors,
	m	The number of DM points.
Return:	A	The matrix of Basis functions,
	B	The DM vectors (ΔD) captured in matrix form,
	I	An index matching lattice vertices to columns of A,
	n	the length of I and number of columns in A.
Data Structures:	(i, j, k)	Indices of a lattice cell,
	(u, v, w)	Co-ordinates within a lattice cell.

set I to empty
$n \longleftarrow 0$
FOR $\alpha = 1, 2, \ldots, m$
  (1) Parametrise D_α, finding the cell address (i, j, k) and local co-ordinates (u, v, w) in V.
  (2) Assign the vector components of ΔD_α to $B_{\alpha,1}$, $B_{\alpha,2}$, $B_{\alpha,3}$
  FOR $r = 0, \ldots, 3$
    FOR $s = 0, \ldots, 3$
      FOR $t = 0, \ldots, 3$
        Find the position (β) of $(i + r, j + s, k + t)$ in I
        IF not found THEN
          $n \longleftarrow n + 1$
          $\beta \longleftarrow n$
          $I_n \longleftarrow (i + r, j + s, k + t)$
        $A_{\alpha,\beta} \longleftarrow B^3_r(u) \cdot B^3_s(v) \cdot B^3_t(w)$

2.4 Concluding Remarks

The foundations of Directly Manipulated Free-Form Deformation (DMFFD), a sophisticated sculpting tool, have been established. The approach carries considerable benefits:

- **Aesthetic.** Deformations are moulded and tapered due to the Uniform Rational B-Spline substrate. This imparts a fluid clay-like consistency to the solid being modelled and reinforces the sculpting metaphor.
- **Intuitive.** The "Pick-and-Drag" interface that Direct Manipulation overlays on Free-Form Deformation is simple and effective.
- **Local Control.** The extent of deformations is dependent on the size and spread of the FFD lattice. A fine lattice allows intricate, detailed deformation, while a coarse lattice is needed for global changes.
- **Representation Independence.** Finding surface points is fundamental to all representation schemes. Since FFD is point-based it is independent of the formulation of its embedded solid [Sederberg and Parry 1986].

However, inefficiency remains a worrisome consideration, despite the range of improvements presented thus far. The kernel of computation in DMFFD is the reverse-engineering of the lattice and this is addressed in the next chapter.

Chapter 3

Least Squares Solution Methods

At this juncture the foundations of Directly Manipulated Free-Form Deformation are in place. However, the core computation, a reverse-engineering of lattice vertices, remains to be considered. It is this calculation that is the principal source of inefficiency in DMFFD.

In the previous chapter DMFFD was considered in terms of the relationship between three matrices: a basis matrix of spline weights (A), a matrix of lattice vertex co-ordinates (X), and a matrix of altered object points (B). In this chapter these matrices are arranged into a system of linear equations $AX = B$ and the problem is reduced to finding X, given A and B, using a construction known as the Pseudo-inverse. These theoretical underpinnings are discussed in the next section, culminating in a concise statement of the problem.

The bulk of the chapter is devoted to a discussion of four methods for solving this problem: the Naïve Pseudo-inverse [Noble 1969], Normal Equation [Lawson and Hanson 1974], Greville [Greville 1960] and Householder [Lawson and Hanson 1974] schemes. These approaches are outlined and compared with regard to efficiency, accuracy and space consumption. Here efficiency is measured as the number of multiplications and divisions required by an algorithm. Additions and subtractions are ignored in this evaluation since they are of a similar order to, and consume less computation time than, multiplications and divisions. Space consumption is measured as the amount of floating point storage over and above that required for A, X and B. Finally, in considering accuracy, the degeneration in the significant digits of the solution X relative to the matrix B is measured.

The remainder of the chapter focuses on selecting one numerical scheme for DMFFD according to these measures. An effective and novel enhancement is then made to the chosen scheme by exploiting the structure of the basis matrix (A). Finally, this improved DMFFD algorithm is presented in its entirety and its efficiency demonstrated.

3.1 Theoretical Underpinnings

3.1.1 Systems of Linear Equations

Direct Manipulation of Free-Form Deformation may be posed in terms of solving a system of linear equations. Such systems are traditionally written in **matrix** notation as $Ax = b$. Here A is an $m \times n$ matrix of coefficients and x and b are n-dimensional and m-dimensional column vectors respectively. Both A and b are predetermined and the problem involves finding solution values for the set of unknowns x.

This process is very well-defined when A is square ($m = n$) and **non-singular**, that is an inverse denoted by A^{-1} exists. This inverse is constructed so that x can be solved explicitly as $x = A^{-1}b$. If the right-hand-side vector b is altered, a corresponding solution x can be found without re-evaluating A^{-1}. The inverse provides a theoretical underpinning for a plethora of solution methods.

Less well documented are solutions to **underdetermined** and **overdetermined** systems. In the former case there are more unknowns than equations ($m < n$ in A) and one or more of the unknowns becomes free or variable, spawning an infinite number of solutions. In the latter case there are more equations than unknowns ($m > n$ in A) and there is no exact solution, since not all of the constraints can be met.

A further complication is the **rank** of A. This can be defined as the dimension of the row space of A [Johnson *et al* 1993]. In concrete terms this is equivalent to the number of nonzero rows that A has after it is reduced to row echelon form. Two further exigencies must now be considered: A may have full rank ($Rank(A) = m$) so that every row contributes constraints, or be rank deficient ($Rank(A) < m$) if some rows of A are linear combinations

of others. Further, if A is rank deficient, so that one row is a constant multiple of another, and the same relationship does not hold in corresponding entries of b then the system is **inconsistent.** More strictly, consistency implies that the same linear dependence relations that hold in A must also hold in b. If a rank deficient system is consistent then one or more rows are redundant.

So, four classes of linear systems have been introduced: full rank underdetermined, rank deficient underdetermined, full rank overdetermined, and rank deficient overdetermined systems. None of these systems have solutions in the traditional sense of a single numerical match for every entry of x. Overdetermined systems allow only approximate solutions and underdetermined systems have an infinity of available solutions. In the overdetermined case, a vector which minimizes the sum of squares (or **norm**) of the residual error ($||Ax - b||$) is considered ideal [Lawson and Hanson 1974] since it is closest in a least squares sense to an exact solution. In the underdetermined case a solution is selected to minimize the sum of squares of the solution vector ($||x||$) and this corresponds to finding the closest solution to the zero vector.

Direct Manipulation can be posed in terms of the underdetermined full rank least squares problem, which can be simply stated:

The Underdetermined Full Rank Least Squares Problem
Minimize $||x||$ (or equivalently $x^T x$) subject to $Ax = b$
where $A \in \mathcal{U}^{m \times n}$, $x \in \Re^n, b \in \Re^m$
and $\mathcal{U}^{m \times n}$ is the underdetermined $m \times n$ matrix space defined by
$\mathcal{U}^{m \times n} \subset \Re^{m \times n}$, $Rank(\mathcal{U}^{m \times n}) = m$ and $m < n$.

3.1.2 The Pseudo-inverse

The Pseudo-inverse, represented by A^+, extends the definition of the inverse A^{-1} to under- and overdetermined situations. Many of the properties of the inverse carry over in this generalization. For instance, A^+ is dependent solely on the coefficient matrix A. The explicit solution $x = A^+ b$ coincides with the normal interpretation when A is square (ie.

$A^+ = A^{-1}$), the solution vector with minimum norm when A is underdetermined, and the norm of the residual error when A is overdetermined. The Pseudo-inverse thus solves the underdetermined full rank least squares problem under consideration and can be evaluated using the following result [Noble 1969]:

Theorem 3.1 *[Noble 1969] For $A \in \mathcal{U}^{m \times n}$ the solution of the equation $Ax = b$ that minimizes $x^T x$ is $x = A^+ b$, where the Pseudo-inverse A^+ is the unique $n \times m$ matrix given by $A^+ = A^T(AA^T)^{-1}$.*

Proof [Noble 1969]

The Method of Lagrange Multipliers states that minimizing $g(x)$ subject to $h(x) = 0$ is equivalent to minimizing the Lagrange multiplier $M = g(x) + \lambda h(x)$.

This method is employed to minimize $x^T x$ subject to $Ax = b$. We form $M = x^T x + 2\lambda^T(Ax - b)$, where λ is an $1 \times m$ row vector of Lagrange multipliers with the factor 2 introduced for convenience.

This has a minimum when $\frac{\partial M}{\partial x_i} = 0 \qquad i = 1, \ldots, n$

$\frac{\partial M}{\partial x} = 2x^T - 2\lambda^T A = 0$

$\Rightarrow x^T = \lambda^T A$

$\Rightarrow (x^T)^T = (\lambda^T A)^T$

$\Rightarrow \boxed{x = A^T \lambda}$ ..... (i)

and $\frac{\partial M}{\partial \lambda_j} = 0 \qquad j = 1, \ldots, m$

$\frac{\partial M}{\partial \lambda} = 2(Ax - b) = 0$

$\Rightarrow \boxed{Ax = b}$ ..... (ii)

Now substitute (i) into (ii) to obtain

$AA^T \lambda = b$

$\Rightarrow \lambda = (AA^T)^{-1} b$ (since AA^T is nonsingular)

Substituting this expression for λ into (i) yields

$x = A^T(AA^T)^{-1} b$ as required.

Property 3.2 *The Pseudo-inverse of a row vector v is $v^+ = \|v\|^{-2} v^T$.*

Proof

We have

$$vv^T = \sum_{i=1}^{n} v_i^2 = \|v\|^2$$
$$\Rightarrow (vv^T)^{-1} = \frac{1}{\|v\|^2}$$
$$\Rightarrow v^+ = v^T(vv^T)^{-1} = \frac{1}{\|v\|^2} v^T$$

Property 3.3 *If $AX = B$ with $A \in \mathcal{U}^{m \times n}$, $X \in \Re^{n \times p}$, $B \in \Re^{m \times p}$ and $X = A^+B$ then every column of X is a least squares solution to a system formed with corresponding columns of B.*

Proof

[1] Each column of B is an $m \times 1$ column vector b_i, $i = 1, \ldots, p$ and each column of X is an $n \times 1$ column vector x_i, $i = 1, \ldots, p$.

[2] Now $X = A^+B$ is equivalent to $x_i = A^+b_i$, $i = 1, \ldots, l$ from the definition of matrix multiplication.

[3] By Theorem 3.1 each x_i is a least squares solution to the underdetermined full rank least squares problem.

The central problem of DMFFD can now be stated:

Direct Manipulation Problem Statement
If $AX = B$ and $A \in \mathcal{U}^{m \times n}$, $X \in \Re^{n \times p}$ and $B \in \Re^{m \times p}$ then a solution equivalent to $X = A^+B$ must be found.

3.2 Solution Schemes

3.2.1 Naïve Pseudo-inverse

The unknown matrix X can be naïvely found by a brute-force construction of the Pseudo-inverse A^+. From Theorem 3.1 we get $X = A^T(AA^T)^{-1}B$. Here $C = AA^T$ is inverted by the method of Gauss Reduction with backward substitution on an augmented matrix (see figure 3.2) familiar from elementary linear algebra [Burden and Faires 1993]. The inverse, while useful in theoretical contexts, is avoided in practical applications since it carries a heavy computation overhead (notice the m^3 term contributed by the inversion in the efficiency analysis of Figure 3.1). Later methods will circumvent this inversion in the interests of speed.

Figure 3.1: Analysis of the Naïve Pseudo-inverse

Efficiency:	[1] m^2n
	[2] $m^3 + \frac{1}{2}m^2 - \frac{1}{2}m$
	[3] m^2n
	[4] mnp
	$= \boxed{2m^2n + m^3 + mnp}$
Extra Space:	$C + D + E$
	$= m^2 + m^2 + mn$
	$= \boxed{2m^2 + mn}$

Figure 3.2: Naïve Pseudo-inverse

Purpose: Find a Least Squares Solution to $AX = B$
by the Naïve Pseudo-inverse method
derived from [Hsu *et al* 1992, Burden and Faires 1993].

Given: A, B Matrices of $m \times n$ and $m \times p$ dimensions

Return: X An $n \times p$ solution matrix.

Data Structures: C, D, E Matrices of $m \times m$, $m \times m$ and $n \times m$ dimensions respectively.

[1] $C \longleftarrow AA^T$

[2] *(find $D = C^{-1}$ explicitly and inefficiently by Gauss-Reduction with partial pivoting on an augmented matrix)*
$D \longleftarrow I$
FOR $h = 1, 2, \ldots, m$
IF $C_{h,h} = 0$ THEN *(pivot element is zero)*
$\lambda \longleftarrow 0$
FOR $i = h+1, h+2, \ldots, m$
IF $C_{i,h} > \lambda$ THEN
$\lambda \longleftarrow C_{i,h}$
$swp \longleftarrow i$
IF $\lambda = 0$ THEN
ERROR: matrix C is singular
ELSE
Exchange rows h and swp in C and D

FOR $i = h+1, h+2, \ldots, m$ *(clear column)*
$r \longleftarrow -C_{i,h}/C_{h,h}$
FOR $j = h+1, h+2, \ldots, m$
$C_{i,j} \longleftarrow C_{i,j} + rC_{h,j}$
FOR $j = 1, 2, \ldots, h$
$D_{i,j} \longleftarrow D_{i,j} + rD_{h,j}$

FOR $h = m, m-1, \ldots, 1$ *(backward substitution)*
FOR $i = m, m-1, \ldots, 1$
$$D_{i,h} \longleftarrow D_{i,h} - \sum_{j=i+1}^{m} C_{i,j} D_{j,h}$$
$D_{i,h} \longleftarrow D_{i,h}/C_{i,i}$

[3] $E \longleftarrow A^T D$
[4] $X \longleftarrow EB$

3.2.2 Method of Normal Equations

The method of Normal Equations sidesteps explicit inversion by exploiting two structural properties of $C = AA^T$: [1] C is **symmetric** and [2] C is **non-negative definite** since it is symmetric and $x^TCx \geq 0$ [Lawson and Hanson 1974]. These two attributes are requirements for Choleski Factorization [Burden and Faires 1993], a powerful technique for solving square linear systems and implicitly building the inverse. Under the Method of Normal Equations calculation of $X = A^+B = A^T(AA^T)^{-1}B$ is subdivided into 3 steps (see Figure 3.4):

1. $C = AA^T$ by matrix multiplication of the lower triangle and using symmetry to build the remainder of C.
2. $D = C^{-1}B$ by Choleski Factorization
3. $X = A^TD$ by matrix multiplication

The consequent improvement in speed is roughly fourfold as can be seen by comparing Figure 3.1 and Figure 3.3.

Figure 3.3: Analysis of Method of Normal Equations

Efficiency:
[1] $\frac{1}{2}m^2n$
[2] $\frac{1}{6}m^3 + \frac{1}{2}m^2 - \frac{2}{3}m + m$ sqrts [Burden and Faires 1993]
[3] $m^2p + mp$ [Burden and Faires 1993]
[4] mnp
$= \boxed{\frac{1}{2}m^2n + \frac{1}{6}m^3 + m^2p + mnp}$

Extra Space:
$C + L + y + D$
$= m^2 + \frac{1}{2}m^2 + m + mp$
$= \boxed{\frac{3}{2}m^2 + m + mp}$

Accuracy:
This is proportional to the square of the **condition number** of A [Golub and Van Loan 1989]

Figure 3.4: Method of Normal Equations

Purpose: Find a Least Squares Solution to $AX = B$ by the Method of Normal Equations with a Choleski Factorization found in [Burden and Faires 1993].

Given: A, B Matrices of $m \times n$ and $m \times p$ dimensions.

Return: X An $n \times p$ solution matrix.

Data Structures: C, D, L Matrices of $m \times m$, $\frac{1}{2}m \times \frac{1}{2}m$ and $m \times p$ dimensions respectively.

[1] *(form* $C \longleftarrow AA^T$*)*

FOR $i = 1, 2, \ldots, m$ *(standard matrix multiplication of lower triangle)*

FOR $j = 1, 2, \ldots, i$

$$C_{i,j} \longleftarrow \sum_{k=1}^{n} A_{i,k} A_{j,k}$$

IF $i \neq j$ THEN $C_{j,i} \longleftarrow C_{i,j}$ *upper triangle mirrors lower*

[2] *(find a lower triangular factorization* L *by Choleski Decomposition)*

$$L_{1,1} \longleftarrow \sqrt{C_{1,1}}$$

FOR $j = 2, 3, \ldots, m$

$$L_{j,1} \longleftarrow C_{j,1}/L_{1,1}$$

FOR $i = 2, 3, \ldots, m-1$

$$L_{i,i} \longleftarrow \sum_{k=1}^{i-1} L_{i,k}^2$$

$$L_{i,i} \longleftarrow \sqrt{C_{i,i} - L_{i,i}}$$

FOR $j = i+1, i+2, \ldots, m$

$$L_{j,i} \longleftarrow \sum_{k=1}^{i-1} L_{j,k} L_{i,k}$$

$$L_{j,i} \longleftarrow (C_{j,i} - L_{j,i})/L_{i,i}$$

$$L_{m,m} \longleftarrow \sum_{k=1}^{m-1} L_{m,k}^2$$

$$L_{m,m} \longleftarrow \sqrt{C_{m,m} - L_{m,m}}$$

[3] *(use the Choleski Factorization to solve for* D*)*

FOR $k = 1, 2, \ldots, p$

$$y_1 \longleftarrow B_{1,k}/L_{1,1}$$

FOR $i = 1, 2, \ldots, m$

$$y_i \longleftarrow \sum_{j=1}^{i-1} L_{i,j} y_j$$

$$y_i \longleftarrow (B_{i,k} - y_i)/L_{i,i}$$

$$D_{m,k} \longleftarrow y_m/L_{m,m}$$

FOR $i = m-1, m-2, \ldots, 1$

$$D_{i,k} \longleftarrow \sum_{j=i+1}^{m} L_{j,i} D_{j,k}$$

$$D_{i,k} \longleftarrow (y_i - D_{i,k})/L_{i,i}$$

[4] $X \longleftarrow A^T D$

3.2.3 Greville's Method

A touted alternative to the previous two schemes has been derived [Greville 1960]. Greville's approach relies on a recursive decomposition of the Pseudo-inverse. This requires some additional notation: A_k is the $m \times k$ submatrix encompassing the first k columns of A, A_k^+ is the corresponding $k \times m$ Pseudo-inverse and a_k is the $m \times 1$ vector of the k-th column of A. Now Theorem 3.4 provides a mechanism for successively introducing columns of A and thereby recursively building A^+.

Theorem 3.4 *[Greville 1960] A_k^+, the Pseudo-inverse of the submatrix A_k, is dependent solely on A_{k-1}^+, A_{k-1} and a_k. Their relationship is defined as follows:*

$$A_k^+ = \begin{bmatrix} A_{k-1}^+ - de \\ e \end{bmatrix}$$

where $d = A_{k-1}^+ a_k$

and e is determined by: $c = a_k - A_{k-1} d$

IF $c \neq 0$ *THEN*

$e = c^+$

ELSE IF $c = 0$ *THEN*

$e = (1 + d^T d)^{-1} d^T A_{k-1}^+$

Proof

This proof is too convoluted for presentation here (see [Greville 1960] for details).

Notice that we have a means of evaluating the Pseudo-inverse of a row vector v as $v^+ = \|v\|^{-2} v^T$ (from Property 3.2). This can be applied unchanged to column vectors.

It is now possible to calculate A^+ beginning from A_1^+ (the Pseudo-inverse of the first column of A) and iterating until A_n^+ (the Pseudo-inverse of A) is reached, as is done in figure 3.6.

The analysis of this algorithm (see figure 3.5) contradicts its purported strength [Borrel and Bechmann 1992], especially in the light of its inefficiency. However, the method has two redeeming attributes:

- Column **Updating** and **Downdating** of A does not force a complete recalculation of the Pseudo-inverse A^+. Unfortunately Direct Manipulation is row oriented in this respect and only ever requires adding or removing rows of A.
- The algorithm is independent of the relative dimensions of m and n in A so that it can be applied unchanged to both the under- and overdetermined cases.

Figure 3.5: Analysis of Greville's Method

Efficiency:
$[1]\ 2m$
$[2]\ mn^2 - mn$
$[3a]\ 2mn - 2m$ OR
$[3b]\ \frac{1}{2}mn^2 - \frac{1}{2}mn + mn - m + n^2 - n$
$[4]\ \frac{1}{2}mn^2 - \frac{1}{2}mn$
$[5]\ mnp$
$= \boxed{\frac{3}{2}mn^2 + mnp}$

Extra Space:
$P + a + c + d + e$
$= mn + m + n + m + m$
$= \boxed{mn + 3m + n}$

Figure 3.6: Greville's Method

Purpose: Find a Least Squares Solution to $AX = B$ by Greville's Method found in [Greville 1960].

Given: A, B Matrices of $m \times n$ and $m \times p$ dimensions.

Return: X An $n \times p$ solution matrix.

Data Structures: P An $n \times m$ Matrix which stores the partial pseudo-inverse

a,c,d,e intermediate vectors

[1] *(find the Pseudo-inverse of column 1 of A)*

$\lambda \longleftarrow 1/\sum_{i=1}^{m}(A_{i,1})^2$

FOR $i = 1, 2, \ldots, m$

$P_{1,i} \longleftarrow \lambda A_{i,1}$

$P_{row} \longleftarrow 1$

(iterative calculation of $P = A_k^+$)

FOR $k = 2, 3, \ldots, n$

[2] FOR $i = 1, 2, \ldots, m$

$a_i \longleftarrow A_{i,k}$

$d \longleftarrow Pa$

$A_{col} \longleftarrow k - 1$ *(A set temporarily to A_{k-1})*

$c \longleftarrow Ad$

FOR $i = 1, 2, \ldots, m$

$c_i \longleftarrow a_i - c_i$

[3a] IF $c \neq 0$ THEN

$e \longleftarrow \frac{1}{\|c\|^2} c$

[3b] ELSE $(c = 0)$

$\alpha \longleftarrow 1/(1 + \sum_{i=1}^{n} d_i^2)$

$e \longleftarrow \alpha d^T P$

[4] *(determine A_k^+)*

FOR $i = 1, 2, \ldots, k - 1$

FOR $j = 1, 2, \ldots, m$

$P_{i,j} \longleftarrow P_{i,j} - d_i e_j$

$P_{row} \longleftarrow P_{row} + 1$

FOR $j = 1, 2, \ldots, m$

$P_{k,j} \longleftarrow e_j$

[5] $X \longleftarrow PB$

3.2.4 Householder QR Factorization

There is an alternative characterization of the Pseudo-inverse which is based on an **orthogonal** decomposition of A and which leads to an effective numerical scheme for least squares solutions. Briefly a matrix Q is orthogonal if $Q^TQ = I$. An orthogonal matrix Q has the property of preserving Euclidian length under multiplication, thus $\|Qy\| = \|y\|$.

We are now in a position for an alternative definition of the Pseudo-inverse.

Theorem 3.5 *[Lawson and Hanson 1974] Let $A \in \mathcal{U}^{m\times n}$. Given an orthogonal decomposition $A = H \begin{bmatrix} R & 0 \end{bmatrix} K^T$, where $H \in \Re^{m\times m}$ and $K \in \Re^{n\times n}$ are orthogonal and $R \in \Re^{m\times m}$, then the Pseudo-inverse is given by:*

$$A^+ = K \begin{bmatrix} R^{-1} \\ 0 \end{bmatrix} H^T$$

A^+ is uniquely defined by A, and does not depend on the orthogonal decomposition of A.

It is important to remember that finding the inverse of a square, upper or lower triangular matrix is particularly simple since it is already in row echelon form and the computationally demanding Gauss Reduction step can be bypassed. So an orthogonal decomposition which leaves R in this form is ideal. Such a decomposition is called a QR factorization.

Theorem 3.6 *[Lawson and Hanson 1974] If $A \in \mathcal{U}^{m\times n}$ then there exists a factorization of A such that $A = I_m \begin{bmatrix} R & 0 \end{bmatrix} Q^T$ where Q is orthogonal and R is zero above the main diagonal.*

Notice that the decomposition $A = I_m \begin{bmatrix} R & 0 \end{bmatrix} Q^T$ satisfies all the conditions of theorem 3.5 so that $A^+ = Q \begin{bmatrix} R^{-1} \\ 0 \end{bmatrix} I_m$. An implicit algorithm for finding X, given the QR orthogonal decomposition of theorem 3.6, can now be derived.

Derivation of figure 3.8

$$\begin{aligned} A &= I_m \begin{bmatrix} R & 0 \end{bmatrix} Q^T \\ \Rightarrow AQ &= \begin{bmatrix} R & 0 \end{bmatrix} Q^TQ \\ \Rightarrow AQ &= \begin{bmatrix} R & 0 \end{bmatrix} I \quad \text{(Q is orthogonal and so } Q^TQ = I\text{)} \end{aligned}$$

[1] $\boxed{AQ = \begin{bmatrix} R & 0 \end{bmatrix}}$

$$X = A^{+}B$$
$$\Rightarrow X = Q \begin{bmatrix} R^{-1} \\ 0 \end{bmatrix} B \quad \text{(by theorem 3.5)}$$
$$\Rightarrow X = Q \begin{bmatrix} R^{-1}B \\ 0 \end{bmatrix} \quad \text{(block multiplication)}$$

[2] $\boxed{\text{solve for } Y \text{ in } RY = B}$

[3] $\boxed{X = Q \begin{bmatrix} Y \\ 0 \end{bmatrix}} \quad (Y = R^{-1}B)$

Further, there exists a stable method for determining Q known as the Householder Factorization [Lawson and Hanson 1974] which is used frequently in eigenvalue problems. It is presented here without derivation.

Figure 3.7: Analysis of Householder QR Factorization

Efficiency:	[1] $mn - \frac{1}{2}m^2 + m - n$ [2] $m^2n + m^2 - \frac{1}{3}m^3 - mn - \frac{2}{3}m$ [3] $\frac{1}{2}m^2p - \frac{1}{2}mp + mp - p$ [4] $2mnp - m^2p + 2mp - 2np$ $= \boxed{m^2n - \frac{1}{3}m^3 - \frac{1}{2}m^2p + 2mnp}$
Extra Space:	$Y + h$ (Q, R are stored over A except for h) $= \boxed{mp + n}$
Accuracy:	This is proportional to the Condition Number of A [Golub and Van Loan 1989]

Figure 3.8: Householder QR Factorization

Purpose:	Find a Least Squares Solution to $AX = B$	
	by Householder QR Factorization	
	found in [Lawson and Hanson 1974].	
Given:	A, B	Matrices of $m \times n$ and $m \times p$ dimensions.
Return:	X	An $n \times p$ solution matrix.
Data		
Structures:	Q	A Householder Decomposition
	Y, R	intermediate matrices

[1] Create Q – Householder Decomposition

[2] $R \longleftarrow AQ$ *(apply householder decomposition)*

[3] *(solve for* $RY = B$*)*

FOR $k = 1, \ldots, p$

$Y_{1,k} \longleftarrow B_{1,k}/A_{1,1}$

FOR $i = 2, 3, \ldots, m$

$$Y_{i,k} \longleftarrow B_{i,k} - \sum_{j=1}^{i-1} R_{i,j} Y_{j,k}$$

$$Y_{i,k} \longleftarrow Y_{i,k}/R_{i,i}$$

$(X = [\ Y \quad 0\ ])$

FOR $i = 1, 2, \ldots, m$

$X_{i,k} \longleftarrow Y_{i,k}$

FOR $i = m+1, m+2, \ldots, n$

$X_{i,k} \longleftarrow 0$

[4] $X \longleftarrow QX$ *(apply householder decomposition to* X*)*

Figure 3.9: Comparison of Numerical Schemes

	Efficiency	*Extra Space*
Naïve Pseudo-inverse	$2m^2n + m^3 + mnp$	$2m^2 + mn$
Normal Equations	$\frac{1}{2}m^2n + \frac{1}{6}m^3 + m^2p + mnp$	$\frac{3}{2}m^2 + m + mp$
Greville	$\frac{3}{2}mn^2 + mnp$	$mn + 3m + n$
Householder	$m^2n - \frac{1}{3}m^3 - \frac{1}{2}m^2p + 2mnp$	$mp + n$

3.2.5 Evaluation

In selecting an underdetermined least squares solution scheme, Greville's Method and the Naïve Pseudo-inverse can be dismissed. The Naïve Pseudo-inverse is in all ways an inferior version of the Method of Normal Equations, and Greville's Method excels only in a column updating/downdating situation where A remains largely unaltered. As is apparent from Figure 3.9, only the Method of Normal Equations and Householder QR Factorization are serious contenders.

Householder QR factorization has two main advantages:

1. It is a stable and accurate scheme and can thus be applied to a broader, more **poorly-conditioned** class of matrices [Golub and Van Loan 1989]. Also the resolution of the solution matrix X will not be markedly inferior to that of the right-hand-side matrix B.

2. It is a remarkably compact approach since most intermediate steps of the algorithm overwrite entries of the coefficient matrix A. This does not, however, apply to a sparse matrix structure where zero entries of A are stored implicitly. Paradoxically the Normal Equation method is stronger here. **For example:** Assume that A has $\frac{2}{10}$

density (ie. 20% of matrix entries are nonzero) and dimensions $m = 10$, $n = 100$ and $p = 1$. Then the Method of Normal Equations and Householder QR Factorization will require $\frac{3}{2}m^2 + 2m = 170$ and $\frac{8}{10}mn + m + n = 910$ extra floating-point storage respectively. This occurs because the Householder scheme requires that A be expanded into an explicit form.

The Method of Normal Equations has an edge in efficiency over Householder QR Factorization. The literature claims that it is twice as efficient [Lawson and Hanson 1974] but this is only true when n is far larger than m ($n \gg m$) because then the m^3 term in the efficiency expression (refer to figure 3.9) becomes relatively insignificant. Accuracy considerations (we need η^2 precision to get the accuracy that Householder QR Factorization could achieve with η precision [Lawson and Hanson 1974]), mean that this method must rely on well-conditioned matrices.

In the final analysis the tradeoff is between the requirements of efficiency, in which the Method of Normal Equations is paramount, and space and accuracy, where Householder QR Factorization is preferable.

3.3 Direct Manipulation Specifics

At this stage, a least squares scheme is selected from those outlined and Direct Manipulation specific enhancements are made to it. Finally, these improvements are incorporated in a complete Direct Manipulation algorithm whose superior performance is demonstrated.

DMFFD corresponds exactly to a least squares solution of an underdetermined linear system. The nuances of this equivalence can be summarized as follows:

Given a system of linear equations $AX = B$ where

B is an $m \times p$ matrix of direct manipulation vectors,

X is an $n \times p$ matrix of change vectors for lattice control vertices,

A is an $m \times n$ basis matrix with spline coefficients that give weighting to entries of X,

m is the number of directly manipulated (DM) points on the models surface (between 0 and 64),

n is the number of influenced lattice vertices
(ranging from 64 clustered around a single cell to potentially
over 4000 if DM points are widely scattered across the lattice), and

p the number of axes in the modelling application (3-dimensional in this case).

Direct Manipulation aims to reverse-engineer X from values of A and B.

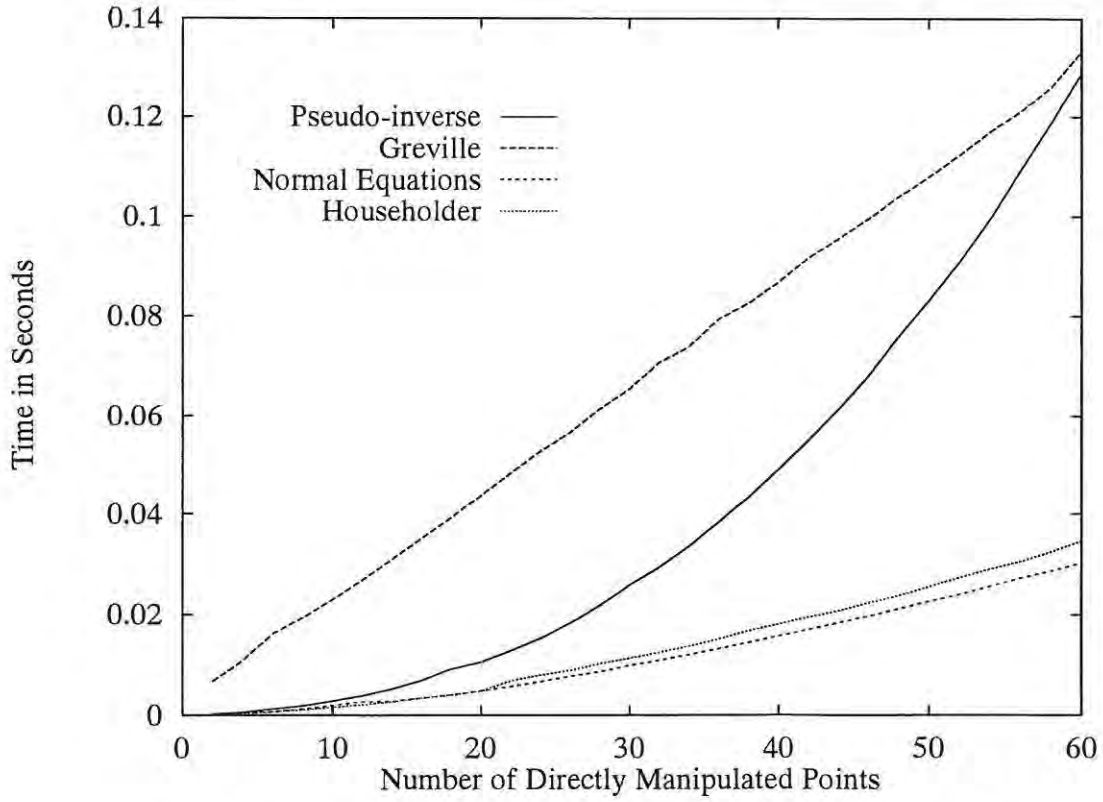

Figure 3.10: An Efficiency Comparison of Least Squares Methods

In determining the required alteration in lattice vertices dictated by X, efficiency is the primary concern and space consumption and accuracy are of secondary importance. As long as they remain within generous limits they are subsumed in the interests of real-time performance. With this in mind Figure 3.10 is a speed-based comparison of the four approaches of the previous section in a representative Direct Manipulation context. The methods were executed on a SPARCserver 10. All the directly manipulated points (m ranging from 1 to 60 along the x-axis) are concentrated in a single cell (n is fixed at 64). As expected, the Naïve Pseudo-inverse and Greville's Method perform poorly. Less predictably perhaps, the Method of Normal Equations does not differ markedly from

Householder QR Factorization. These results are not anomalous however, since they can be arrived at independently via efficiency analysis. In order for a significant divergence to occur between the two methods n must be an order of magnitude greater than m.

On the basis of this comparison the Method of Normal Equations is chosen over and above the other schemes. However, the performance of this approach remains disturbing. **For example:** 60 DM points seeded across 10 adjacent cells requires at least 0.132 seconds to evaluate. This is equivalent, without even accounting for rendering overhead, to 7.6 frames per second, which is considerably below the interactivity cutoff of 15 frames per second. To maintain real-time response, either the number of cells, or the number of directly manipulated points would have to be severely curtailed, both of which would hamstring the utility of Direct Manipulation.

Figure 3.11: Enhanced Direct Manipulation

Purpose: Reverse-engineer lattice vertices for Direct Manipulation
using the Method of Normal Equations [Lawson and Hanson 1974]
with special-purpose enhancements.

Given:
- V A 3D FFD lattice,
- D A set of Directly Manipulated object points,
- ΔD A set of Direct Manipulation vectors,
- m The number of DM points.

Return: An altered version of the 3D FFD lattice V

Data Structures:
- (i, j, k) Indices of a lattice cell,
- (s, t, u) Co-ordinates within a lattice cell,
- (S, T, U) Spline storage arrays,
- A, B, C, D, L Intermediate Matrices,
- $\mathcal{A}$ Sparse basis matrix
- $\mathcal{A}index$ An index of Lattice Cells corresponding to $\mathcal{A}$

[1] *(create compact basis matrix $\mathcal{A}$ and right-hand-side matrix B)*

$row \longleftarrow 0$
$n \longleftarrow 0$
FOR $\alpha = 1, 2, \ldots, m$
  IF D_α is within the scope of the lattice
    (i) Parametrise D_α, finding the cell address (i, j, k) and
      local co-ordinates (s, t, u) in V.
    (ii) Assign the vector components of ΔD_α to $B_{row,1}$, $B_{row,2}$, $B_{row,3}$
    $\mathcal{A}index_{row,1} \longleftarrow i$
    $\mathcal{A}index_{row,2} \longleftarrow j$
    $\mathcal{A}index_{row,3} \longleftarrow k$
    FOR $a = 1, 2, \ldots, 4$
      $S_a \longleftarrow B_a^3(s)$
      $T_a \longleftarrow B_a^3(t)$
      $U_a \longleftarrow B_a^3(u)$
    FOR $a = 1, 2, \ldots, 4$
      FOR $b = 1, 2, \ldots, 4$
        FOR $c = 1, 2, \ldots, 4$
          $\mathcal{A}_{row,a,b,c} \longleftarrow S_a \times T_b \times U_c$
    $row \longleftarrow row + 1$
$m \longleftarrow row$

[2] *(form the normal equations $C = AA^T$ from $\mathcal{A}$)*

FOR $row = 1, 2, \ldots, m$

FOR $col = 1, 2, \ldots, row$

FOR $dim = 1, 2, 3$

(determine the degree of overlap in the current dimension)

$overlap \longleftarrow \mathcal{A}index_{row,dim} - \mathcal{A}index_{col,dim}$

IF $overlap \in [0, 3]$

$startrow_{dim} \longleftarrow overlap$

$startcol_{dim} \longleftarrow 0$

$extent_{dim} \longleftarrow 4 - overlap$

IF $overlap \in [-1, -3]$

$startrow_{dim} \longleftarrow 0$

$startcol_{dim} \longleftarrow overlap \times -1$

$extent_{dim} \longleftarrow 4 + overlap$

OTHERWISE

$extent_{dim} \longleftarrow 0$

$v \longleftarrow 0$

FOR $a = 1, \ldots, extent_1$

FOR $b = 1, \ldots, extent_2$

FOR $c = 1, \ldots, extent_3$

$v \longleftarrow v + \mathcal{A}_{row,a+startrow_1,b+startrow_2,c+startrow_3} \times \mathcal{A}_{col,a+startcol_1,b+startcol_2,c+startcol_3}$

$C_{row,col} \longleftarrow v$

$C_{col,row} \longleftarrow v$

[3] *(find a lower triangular factorization L by Choleski Decomposition)*

$L_{1,1} \longleftarrow \sqrt{C_{1,1}}$

FOR $j = 2, 3, \ldots, m$

$L_{j,1} \longleftarrow C_{j,1}/L_{1,1}$

FOR $i = 2, 3, \ldots, m-1$

$$L_{i,i} \longleftarrow \sum_{k=1}^{i-1} L_{i,k}^2$$

$L_{i,i} \longleftarrow \sqrt{C_{i,i} - L_{i,i}}$

FOR $j = i+1, i+2, \ldots, m$

$$L_{j,i} \longleftarrow \sum_{k=1}^{i-1} L_{j,k} L_{i,k}$$

$L_{j,i} \longleftarrow (C_{j,i} - L_{j,i})/L_{i,i}$

$$L_{m,m} \longleftarrow \sum_{k=1}^{m-1} L_{m,k}^2$$

$L_{m,m} \longleftarrow \sqrt{C_{m,m} - L_{m,m}}$

[4] *(use the Choleski Factorization to solve for D)*

FOR $k = 1, 2, \ldots, p$

$y_1 \longleftarrow B_{1,k}/L_{1,1}$

FOR $i = 1, 2, \ldots, m$

$$y_i \longleftarrow \sum_{j=1}^{i-1} L_{i,j}\, y_j$$

$y_i \longleftarrow (B_{i,k} - y_i)/L_{i,i}$

$D_{m,k} \longleftarrow y_m/L_{m,m}$

FOR $i = m-1, m-2, \ldots, 1$

$$D_{i,k} \longleftarrow \sum_{j=i+1}^{m} L_{j,i} D_{j,k}$$

$D_{i,k} \longleftarrow (y_i - D_{i,k})/L_{i,i}$

[5] FOR $\alpha = 1, 2, \ldots, m$

FOR $a = 1, 2, \ldots, 4$

FOR $b = 1, 2, \ldots, 4$

FOR $c = 1, 2, \ldots, 4$

$i \longleftarrow \mathcal{A}index_{\alpha,1}$

$j \longleftarrow \mathcal{A}index_{\alpha,2}$

$k \longleftarrow \mathcal{A}index_{\alpha,3}$

$basis \longleftarrow \mathcal{A}_{\alpha,a,b,c}$

assign $D_{\alpha,1}$, $D_{\alpha,2}$, $D_{\alpha,3}$ to *delta*

$V_{i+a-1,j+b-1,k+c-1} \longleftarrow delta$

Fortunately, by exploiting the structure of the basis matrix A, the Method of Normal Equations can be made independent of the number of lattice cells with little consequent overhead. This crucial and novel enhancement is founded in the sparse construction of A and is achieved by delaying the flattening of the 3-dimensional lattice and hence optimizing the formation of $C = AA^T$ (step [1] in Figure 3.4). Each row of A has 64 spline coefficient entries, which are weights for a contiguous $4 \times 4 \times 4$ block of lattice vertices, and the remainder are zero filled. A is a sparse matrix. **For example:** 60 DM points spread across 10 adjacent cells leads to 30.8% density in A. It can thus benefit from compaction. A is replaced by a sparse-matrix structure $\mathcal{A}$, which, for each row, stores the index and 64 spline weights of the lattice block. Originally each i, j entry of $C = AA^T$ was formed by multiplying corresponding entries in row i and j of A and summing across the row. In terms of $\mathcal{A}$, we intersect lattice cubes i and j and sum the multiplied vertices of the overlapping region (step [2] of figure 3.11). After this, the method proceeds as before, until $X = A^T D$ is reached, where allowance must again be made for $\mathcal{A}$. This algorithm appears both in

figure 3.11 and the code of Appendix B.

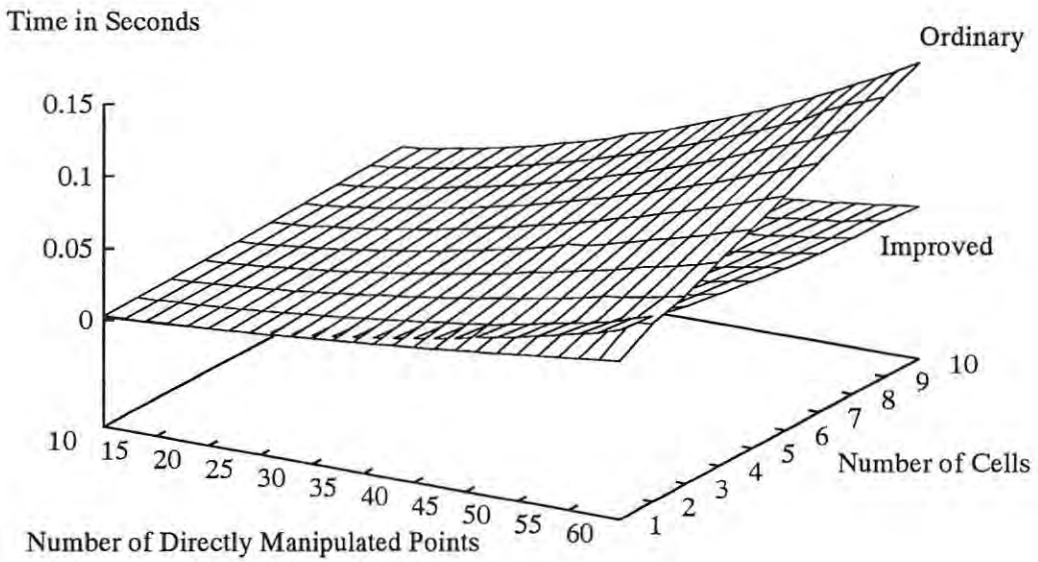

Figure 3.12: Comparison of Ordinary and Improved versions of the Method of Normal Equations for Direct Manipulation across Multiple Cells

Figure 3.12 demonstrates the efficacy of this algorithm. The unenhanced Method of Normal Equations degrades exponentially in both space and time in proportion to the square of the number of cells ($O(cells^2)$). It takes 0.132 seconds with 60 DM points spanning 10 cells. This is by no means an extreme or unrepresentative case.

In contrast the enhanced scheme is independent of the number of cells. It introduces some calculation overhead so that it requires a 2 lattice cell spread to break even. Counter to intuition, performance actually improves as the number of cells increases because lattice cubes overlap less and there are hence fewer multiplications. The costliest operation (reading off Figure 3.12) consumes 0.058 seconds at 60 DM points and a single cell. This is well below the interactivity cutoff.

3.4 Concluding Remarks

A DMFFD algorithm, which combines a new, compact construction of the basis (or coefficient) matrix with a Choleski Factorization of Normal Equations has been developed in this chapter. This is a considerable improvement on the Naïve Pseudo-inverse of the original [Hsu *et al* 1992]. In a representative deformation task, with sixty Direct Manipulation vectors scattered across ten adjacent cells, it increases speed by over an order of magnitude (Naïve Pseudo-inverse = 0.4925s, Enhanced Normal Equations = 0.0365s, Speedup Factor = 13.7). Most importantly, the technique has been made independent (in both speed and time requirements) of the spread of Direct Manipulation vectors across lattice cells.

Chapter 4

Topology and Correctness Issues

This chapter remedies the weaknesses in Directly Manipulated Free-Form Deformation. There are two principal shortcomings that must be addressed: DMFFD can cause self-intersecting shapes by folding a solid through itself, and the smoothness of the Polygon-Mesh degrades under the constant flexing of DMFFD.

These problems and their solutions, are clarified in terms of the topology and correctness of a Polygon-Mesh representation in the subsequent Definition of Terms. This is followed by an investigation of the circumstances under which DMFFD contravenes correctness by engendering self-intersecting solids. Finally refinement (subdividing faces) and decimation (amalgamating faces), two complementary topology-altering schemes which sustain mesh smoothness, are considered.

4.1 Definition of Terms

The terms topology and correctness need to be defined with reference to a Polygon-Mesh representation.

A Polygon-Mesh is built out of vertices, edges and faces. Two vertices serve as the endpoints of an edge, three edges in turn bound a face, and faces surround and enclose the volume of the solid. The whole collection must obey the following rules in order to encode a valid

solid:

1. Euler's Formula must be satisfied:

   $$V - E + F = 2$$

   where V, E and F are, respectively, the number of vertices, edges and faces in the solid.

2. Each edge must connect two vertices.

3. Each edge must be shared by exactly two faces.

4. At least three edges must meet at each vertex.

5. Each face must be formed from a triangle of three edges.

6. Faces must not interpenetrate.

DMFFD is considered correct if it maintains the validity of a solid, as circumscribed by these six rules. The restrictions are slightly more rigorous than required [Foley *et al 1991*], since the fifth rule can be relaxed to encompass more complex polygons. However, a triangle will, by definition, always lie in a plane regardless of the contortion of its vertices. The same does not apply to higher-order polygons.

Topology is the study of the characteristics of mathematical surfaces. It is a rich and varied field, which will receive only cursory treatment here. The primary topological concern in this context is the number and relationship of vertices, edges, faces and holes in a solid. DMFFD is a "tweak" operator [Foley *et al 1991*], which shifts vertices but does not alter the solid's topology: an edge remains an edge, and a face remains a face, no matter how contorted the edge or face becomes. Thus, a solid is said to be **topologically invariant** under Directly Manipulated Free-Form Deformation. This implies that a doughnut can be transformed into a topologically equivalent coffee cup through the agency of DMFFD. Also, this topological invariance preserves the first five rules of validity under DMFFD. It is only the precept that faces must not interpenetrate that may be contravened.

4.2 Self-Intersection

Self-Intersection occurs when a solid is contorted to such an extent that it becomes folded in on itself, with some faces interpenetrating, and the inner surface of the solid partially exposed. Not only is this physically unrealistic but it also undermines the operations that rely on the object's validity. The rendering process, for example, becomes riddled with artefacts and glitches. Unfortunately, solids are prone to self-intersection when acted on by DMFFD, a defect to which the author found no reference. To remedy this, a brief study is made of the different circumstances under which DMFFD spawns self-intersection. This work also prescribes guidelines for avoiding these situations.

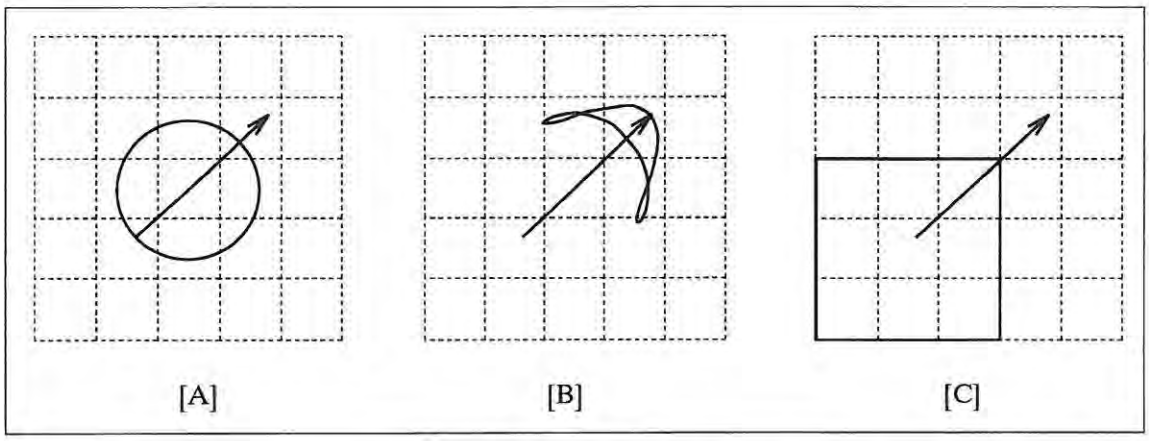

Figure 4.1: Overextension. [A] Initial solid and DM vector, [B] Self-intersection after DMFFD, [C] The DM vector and its zone of immediate influence.

CASE 1: Overextension. Local control is a valuable feature of FFD. It implies that a DM vector anchored in a particular lattice cell will only significantly affect object points in a bounded region surrounding that cell. So, only a limited volume of object points is influenced, but these points may be dragged by the DM vector into undisturbed space outside of this volume. Such an effect is illustrated in figure 4.1 and leads to the following simple prohibition:

Direct-Manipulation vectors may not extend beyond their volume of immediate influence.

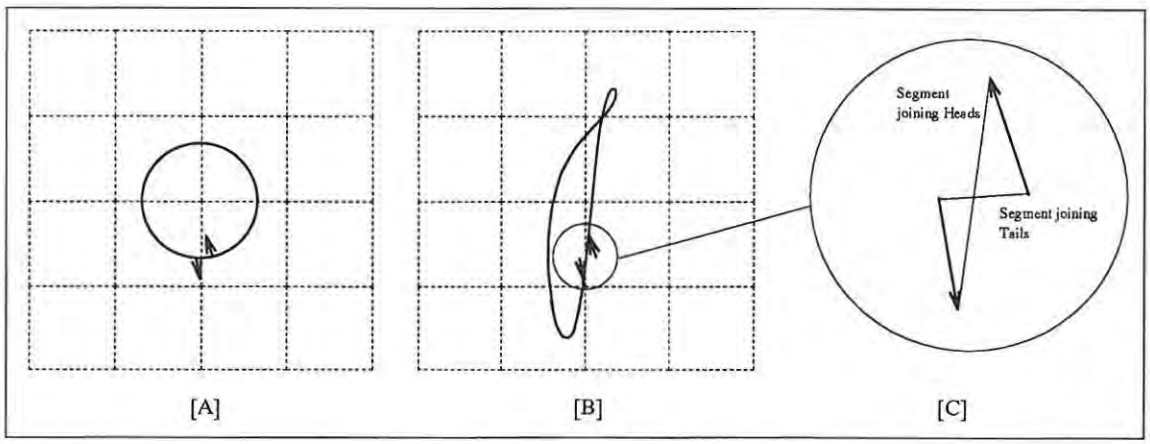

Figure 4.2: Overconstraint. [A] Initial solid and DM vectors, [B] Self-intersection after DMFFD, [C] The DM vectors and their interaction.

CASE 2: Overconstraint. Despite this restriction, object points may still be displaced through unaltered portions of the solid, if DM vectors are steeply constrained. This is evidenced in figure 4.2 where two closely-spaced object points are wrenched in diametrically opposite directions. Self-intersection arises from attempting to interpolate the resulting gradient. These anomalies can be detected as follows: two line segments are formed by joining the heads and the tails of the DM vectors. The slope and length of these segments are then compared. This is summed up in the following principle:

A set of Direct-Manipulation vectors must not constrain object points along too steep a path.

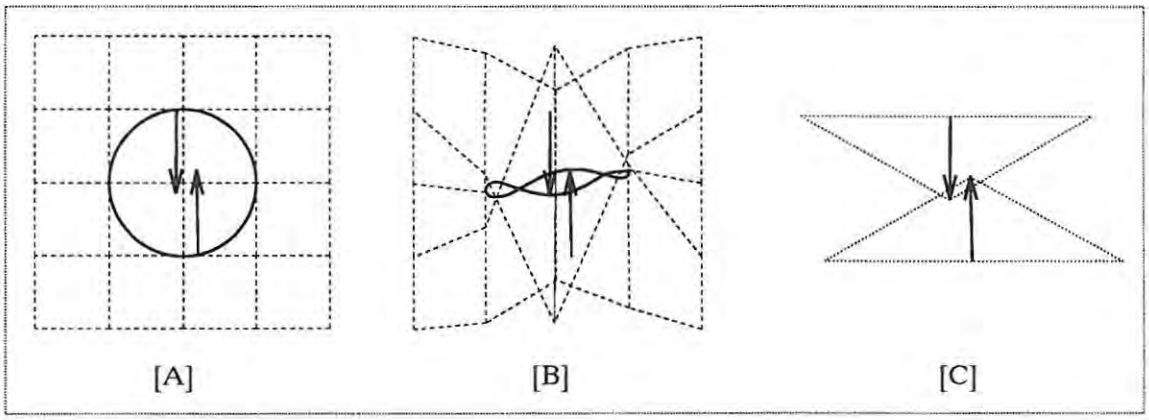

Figure 4.3: Folding. [A] Initial solid and DM vectors, [B] Self-intersection after DMFFD, [C] The DM vectors and their Collision Zones.

CASE 3: Folding. If two or more DM vectors clash they may inadvertently buckle FFD space and generate self-intersection. Two such DM vectors are in conflict (see figure 4.3) if their Collision Zones overlap. The Collision Zone of a vector is a surrounding volume whose extent increases with lattice cell size and the angle between the DM vectors under consideration. For example, the DM vectors of figure 4.3 push in opposite directions and as a consequence have enlarged Collision Zones.

The Collision Zones of two Direct-Manipulation vectors must not overlap.

These three prohibitions are somewhat overexacting and will occasionally exclude a valid set of DM vectors. They are also informal and heuristic and there is scope in this area for further mathematically rigorous research.

4.3 Refinement

The Polygon-Mesh is, by nature, only an approximation of a smoothly sculpted solid. Imagine covering a solid completely with large triangular tiles and then comparing this shell against the original curved and intricate shape. A perfect sphere might, for example, be roughly modelled by an octahedron. The symptoms of an inadequate approximation are a jagged, sharp-edged appearance and the disappearance of smaller features. To compensate, a fine mesh should cover the detailed, highly-curved areas while a coarser mesh spans the remainder of the solid. But even an initially adequate mesh may fail under the contortions of DMFFD. Firstly, DMFFD forcibly stretches the Polygon-Mesh thereby expanding faces and jeopardizing the smoothness of later deformations. Secondly, if the lattice is fine-grained and the directly-manipulated vectors are tightly packed, relative to the size of faces, then the intricacies of the deformation may be forfeit.

For these reasons, an **adaptive refinement** scheme is essential. Adaptive refinement involves recursively subdividing faces in a Polygon-Mesh as required by a deformation. It consists of two tasks: testing a face against some splitting criterion and if necessary tessellating the face according to a subdivision method. Pre- and post-deformation images

of the solid must be maintained. The splitting test is applied to a distorted face while its undistorted version is required for actual subdivision, with new vertices then undergoing deformation.

4.3.1 Splitting Criterion

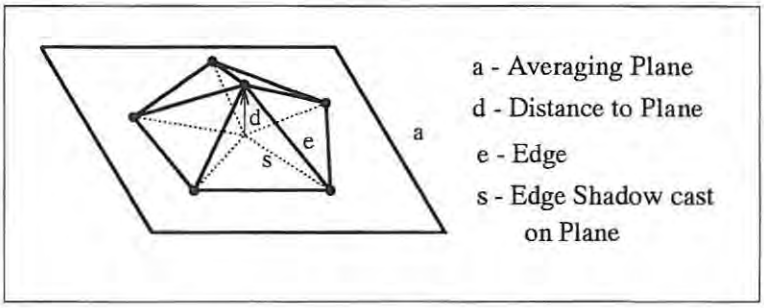

Figure 4.4: The Distance to Averaging Plane Criterion

One measure of the continuity of a portion of the Polygon-Mesh is the angle between adjacent faces: the more acute the angle, the greater the discontinuity. This observation is the basis for a modified distance to averaging plane [Schroeder *et al* 1992] splitting criterion. A central vertex and its loop of adjacent vertices are considered (figure 4.4). A plane which averages the loop is constructed and the distance from this plane to the focal vertex is calculated. Then, the total area of all triangles within the loop is determined. If the ratio of the distance and combined area is above some tolerance then the cycle of triangles is a candidate for refinement. This is only a representative angle-based test; more sophisticated and computationally exorbitant approaches are possible.

However, an elegant heuristic test is preferred. A single triangle is selected and its longest edge compared against the extent of a lattice cell. The face is accepted for subdivision according to the formula:

$$\frac{edgelength}{cellextent} > \frac{1}{4}$$

Edge length is chosen in preference to face area since thin elongated triangles cause discontinuities disproportionate to their surface area. Also, cell extent is measured by the shortest cell edge because lattice cells are parallelpiped and not square. While superfluous

subdivision may sometimes result from this approach, it has the advantages of relying only on information local to a single triangle, a predetermined degree of subdivision and sheer simplicity.

4.3.2 Subdivision Methods

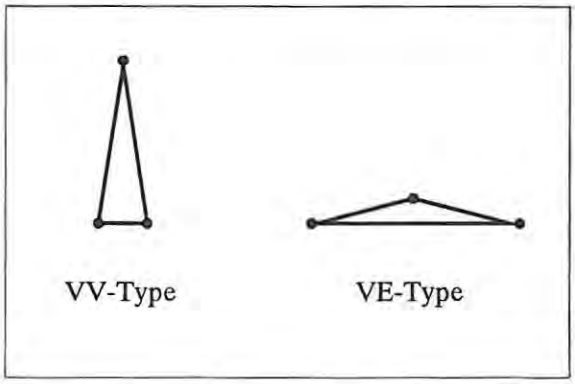

Figure 4.5: Ill-Formed Triangles

A subdivision method, which partitions a triangle or cluster of triangles into smaller elements, must now be considered. Such a method will be selected according to the following attributes:

- **Validity Preservation.** The subdivision must rigorously adhere to the rules prescribing a solid's validity, as outlined previously.
- **Efficiency Conservation.** The subdivision process should be lean and efficient so that the system's interactivity is not hampered. Also, the growth in vertices and faces should be curtailed, since each new vertex must undergo deformation and each new face further burdens rendering.
- **Regular Triangulation.** The formation of thin needle-like triangles should be avoided. There are two classes of ill-formed triangles [Shimada and Gossard 1995]: *vv*-type, where two vertices lie in close proximity and *ve*-type, formed by moving a vertex close to an edge (see figure 4.5). An optimal triangle obeys the Max-Min Angle Principle [Schumaker 1993], which ensures that all angles in a triangle are above a threshold value.

- **Minimal Propagation.** Propagation is the spilling over of subdivision into adjacent faces which is sometimes necessary to enforce triangularity. It may, however, lead to complications if the neighbouring faces in turn require refinement.

These qualities are ranked in descending importance: Validity is crucial while minimal propagation is merely desirable.

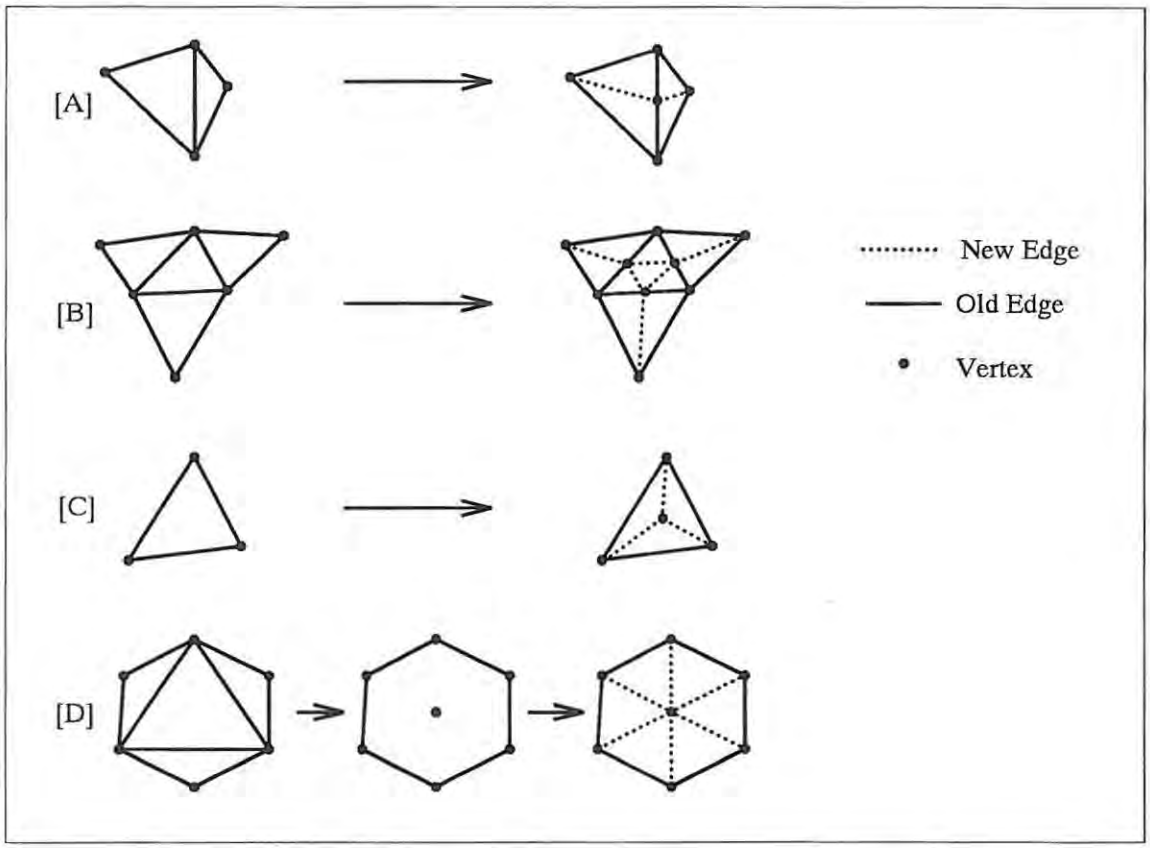

Figure 4.6: Subdivision Methods: [a] Section-Halving, [b] Quaternary Subdivision, [c] Centre Subdivision, [d] Delauney Triangulation.

Four validity preserving subdivision methods are detailed in figure 4.6: Section-Halving, Quaternary Subdivision, Centre Subdivision and Delauney Triangulation. **Section-Halving** [Wördenweber 1983] involves connecting the midpoint of the longest edge to its opposite vertex. A mirroring edge must be placed in the triangle incident on the bisected edge. Thus, a vertex, two edges and two extra faces are introduced, and a single propagation is mandated. In **Quaternary Subdivision** [Bill and Lodha 1994], a triangle is split into four by dividing all the edges and joining the bisection vertices. Propagation under this method

must expand to all adjacent faces. A **Centre Subdivision** [Wördenweber 1983] sets a new vertex in the centre of the triangle, with edges radiating outwards to the corners. There is no subsequent propagation. **Delauney Triangulation** is a powerful approach that imposes an optimal mesh on a cloud of unstructured vertices. It can be harnessed to the current task by first erasing all edges in a bounded portion of the mesh, then placing extra vertices inside this region, and finally applying Delauney Triangulation to remesh the gap.

Of all these methods Delauney Triangulation is the most regular but also the most calculation intensive. Centre Subdivision is the complete opposite: it is highly local and efficient but proliferates narrow triangles. Section-Halving is more moderate but may still generate ill-formed triangles when propagating. In contrast, Quaternary Subdivision functions well in linking subdivisions across a premarked patch of faces. It also conserves efficiency and promotes regularity. For these reasons, Quaternary Subdivision is fused with a Heuristic splitting criterion into an adaptive refinement scheme, which is presented in figure 4.7.

4.4 Decimation

Polygon-Mesh decimation is the antithesis of refinement. Instead of inserting extra vertices, edges and faces, they are whittled away, making the mesh coarser but also less complex. There are several motives for this decimation. Firstly, the adaptive refinement scheme introduced in the previous section is somewhat loose and sacrifices exactitude for efficiency. A consequence is the insertion of superfluous faces which need to be pared away. Secondly, if a mesh is too intricate, this will adversely affect the rendering rate. Sometimes mesh complexity must be sacrificed in the interests of interactivity.

Many of the important properties of refinement apply equally to its complement. However, while validity preservation, regular triangulation and minimal propagation remain vital, efficiency conservation is relegated to a lesser rôle. The efficiency of Polygon-Mesh decimation is not as critical because, unlike refinement, it is not tightly bonded to DMFFD, and can be slotted between bouts of modelling when the system is relatively unencumbered.

Figure 4.7: Adaptive Refinement

Purpose: Check marked faces against a Heuristic Splitting Criterion and if necessary subdivide these faces according to Quaternary Subdivision.

Given:
- $\mathcal{F}$ a face list of n entries with deformed faces marked,
- $\mathcal{V}$ a vertex list,
- *cut* a heuristic constant,
- *cell* the minimum length of a cell.

Return: altered face list $\mathcal{F}$ and vertex list $\mathcal{V}$.

Data Structures:
- $\mathcal{B}$ a bisection list whose entries correspond to faces in $\mathcal{F}$,
- e_1, e_2, e_3 edge vectors of a face,
- v_1, v_2, v_3 vertex indices of a face,
- b_1, b_2, b_3 edge bisectors.

[1] *(Test marked faces against the Heuristic Splitting Criterion)*
FOR $i = 1, \ldots, n$
IF $\mathcal{F}_i$ is marked THEN
Get v_1, v_2, v_3 vertex indices of $\mathcal{F}_i$
$\vec{e_1} \longleftarrow \mathcal{V}_{v_2} - \mathcal{V}_{v_1}$
$\vec{e_2} \longleftarrow \mathcal{V}_{v_3} - \mathcal{V}_{v_2}$
$\vec{e_3} \longleftarrow \mathcal{V}_{v_1} - \mathcal{V}_{v_3}$
$len \longleftarrow$ maximum of $|\vec{e_1}|, |\vec{e_2}|, |\vec{e_3}|$
IF $(len/cell < cut)$ THEN
Unmark $\mathcal{F}_i$
(Now only those faces needing refinement are marked)
[2] *(Subdivide those marked faces that remain)*
FOR $i = 1, \ldots, n$
IF $\mathcal{F}_i$ is marked THEN
IF $\mathcal{B}_{i,1} \neq 0$ THEN
$b_1 \longleftarrow \mathcal{B}_{i,1}$
OTHERWISE
$v \longleftarrow (\mathcal{V}_{v_1} + \mathcal{V}_{v_2})/2$
Place v in the vertexlist $\mathcal{V}$
$b_1 \longleftarrow$ new index of v
... Similarly determine bisectors b_2 of edge v_2v_3 and b_3 of edge v_3v_1
Get v_1, v_2, v_3 vertex indices of $\mathcal{F}_i$
Create new faces $b_1b_2b_3$, $b_1v_2b_2$, $b_2v_3b_3$, $b_3v_1b_1$
Remove $\mathcal{F}_i$
Get adj_1, adj_2, adj_3 indices of faces adjacent to $\mathcal{F}_i$
FOR $k = 1, \ldots, 3$
Get v_1, v_2, v_3 vertex indices of $\mathcal{F}_{adj_k}$
IF b_k bisects v_1v_2 edge THEN
IF adj_k is marked THEN
$\mathcal{B}_{adj_k,1} \longleftarrow b_k$
OTHERWISE
Create new triangles $v_1b_kv_3$, $b_kv_2v_3$
Remove $\mathcal{F}_{adj_k}$
... Similarly check if b_k bisects v_2v_3 or v_3v_1 and either alter $\mathcal{B}$ or split $\mathcal{F}_{adj_k}$ appropriately

Figure 4.8: Deletion Criterion

Purpose: Determine if a loop of triangles requires decimation.
Modified from [Schroeder *et al* 1992].

Given: A loop of triangles with
- $\vec{n_i}$ triangle normals,
- $\vec{x_i}$ triangle centres,
- A_i triangle areas,
- $\vec{V}$ central vertex,
- cut a constant of elimination.

Return: PASS or FAIL on the deletion test.

Data Structures:
- $Area$ total area of the triangle loop,
- $Dist$ distance from the central vertex to the averaging plane,
- $\vec{N}$ averaging plane normal,
- $\vec{X}$ point on the averaging plane.

$Area \longleftarrow \sum A_i$
$\vec{N} \longleftarrow (\sum \vec{n_i}\ A_i)/Area$
$\vec{N} \longleftarrow \vec{N}/|\vec{N}|$
$\vec{X} \longleftarrow (\sum \vec{x_i}\ A_i)/Area$
$Dist \longleftarrow |\vec{N} \cdot (\vec{V} - \vec{X})|$
IF $(Dist/Area) < cut$ THEN
    RETURN PASS
OTHERWISE
    RETURN FAIL

The Polygon-Mesh decimation algorithm is adapted from research into reducing models that are captured from scanned or sampled data [Schroeder *et al* 1992]. The method is fourfold: (1) A vertex is selected, (2) it is tested against a deletion criterion which may trigger (3) the removal of the vertex along with its incident edges and finally (4) the resulting cavity is retriangulated.

The deletion criterion employed in this work is the enhanced distance to averaging plane test, which appeared in the previous section. This was originally [Schroeder *et al* 1992] applied to an evenly-spaced Polygon-Mesh extrapolated from such sources as computed tomography and magnetic resonance scanning, where distance was an adequate measure of angularity. It does not, however, suffice in the presence of adaptive refinement, since this caters for sinuousity of miniscule triangles in a limited locale. This localized convolution will be washed away unless the size of its faces are taken into account, as is done in the

deletion criterion of figure 4.8.

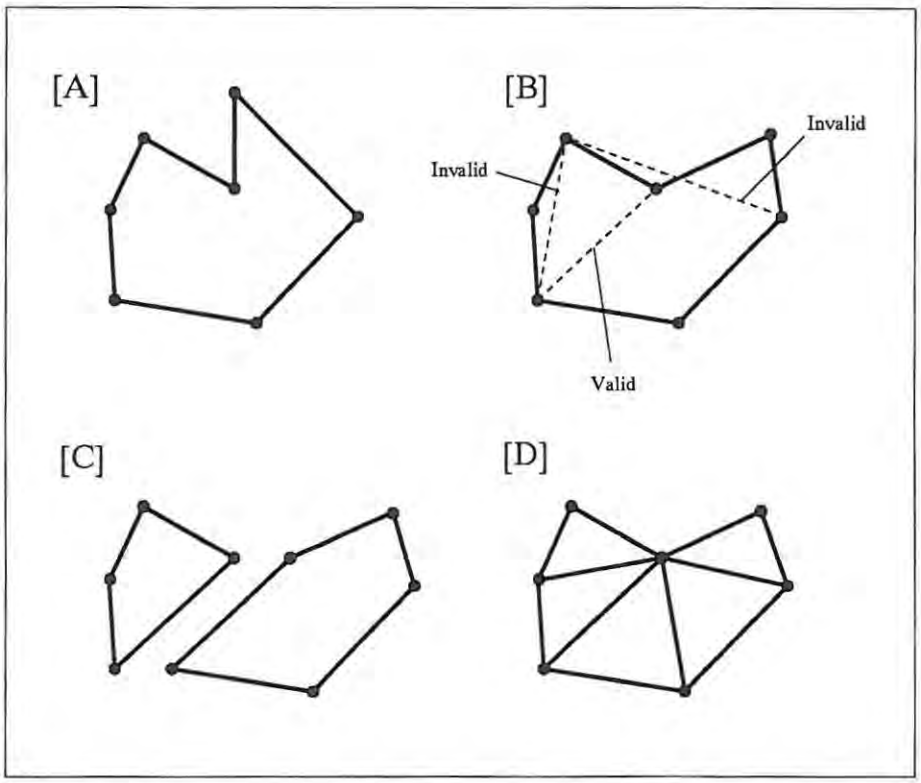

Figure 4.9: Triangulating a Loop: [A] A loop of vertices, [B] Three speculative splits, [C] Subsidiary loops, [D] A final triangulation.

In the final stage of decimation, a non-planar loop of vertices is retriangulated according to a recursive loop splitting procedure [Schroeder *et al* 1992], shown in figure 4.9. At the top level a split line, which joins two non-adjacent vertices and divides the loop in half, is generated. A splitting plane orthogonal to the averaging plane and passing through this split line, is then created. The speculative split becomes an edge in the final triangulation on passing two tests. (1) The two subsidiary loops must fall on opposite sides of the splitting plane. (2) No vertex of either loop should pass too close to the plane or ill-formed triangles will result. Once a split is ratified, the subsidiary loops become candidates for triangulation. This recursion proceeds until every loop is reduced to a triangle. In the event of failure, the decimation procedure backtracks prior to vertex removal and then proceeds to a new vertex. The algorithm associated with this procedure is shown in figure 4.10.

Figure 4.10: Loop Splitting

Purpose: Recursively triangulate a 3D loop of vertices
Extracted from [Schroeder *et al* 1992].

Given: v_k a loop of vertices,
k an ordered set selected from $1, \ldots, m$,
cut a constant of aspect ratio.

Return: FAILURE or
SUCCESS and a list of vertex pairs.

Data Structures: SP a splitting plane,
$T1, T2$ boolean test flags.

```
REPEATEDLY
    Select a new two-element subset (i, j) from k in which:
        (i) i < j,
        (ii) i and j are not consecutive elements in k,
        (iii) i must not be the last element of k while j is the first
    IF this is not possible THEN
        RETURN FAILURE
    OTHERWISE
        Form SP a splitting plane orthogonal to the
        averaging plane and passing through v_i, v_j

        (Test for ill-formed triangles)
        T2 ⟵ TRUE
        FOR p = successive elements of k
            IF (p ≠ i) AND (p ≠ j) THEN
                IF (distance from v_p to SP) / (length of edge v_i − v_j < cut) THEN
                    T2 ⟵ FALSE

        (Test the separation of subsidiary loops)
        T1 ⟵ TRUE
        IF v_p FOR p = successive elements of k from i + 1, ..., j − 1
        are not on one side of SP THEN
            T1 ⟵ FALSE
        IF v_p FOR p = successive elements of k from 1, ..., i − 1 and j + 1, ..., m
        are not on the opposite side of SP THEN
            T1 ⟵ FALSE

        IF T1 AND T2 are both TRUE THEN
            CALL Loop Splitting
                passing (v_p, p = a subset of k from i + 1, ..., j − 1) and
                returning a set of vertex pairs P1
            CALL Loop Splitting
                passing (v_p, p = a subset of k from 1, ..., i − 1 and j + 1, ..., m)
                returning a set of vertex pairs P2
            IF both Loop Splits return SUCCESS THEN
                RETURN SUCCESS along with P1, P2 and (i, j)
```

4.5 Concluding Remarks

Over the span of this chapter, several disturbing failings in DMFFD have been raised and resolved. Categories of self-intersection were identified, and specific restrictions recommended in each case. Subsequently, Refinement and Decimation, two mechanisms for balancing the smoothness and complexity of the Polygon-Mesh, were presented.

Chapter 5

Applications

The preceding chapters presented a correct and efficient free-form sculpting tool. Attention now devolves upon a Virtual Reality interface to support this tool. In this chapter, a Virtual Testbed that uses the RhoVeR (Rhodes Virtual Reality) system is presented and two sculpting applications are discussed: interactive surface sketching, where a solid's shape is captured on computer by tracing a tracker over its surface, and glove-based moulding, where a virtual lump of clay is kneaded by a dataglove-directed virtual hand.

5.1 RhoVeR

The RhoVeR system is intended as a flexible foundation and springboard for designing Virtual Environments. The central premise of the system, in keeping with previous work at Rhodes University [Bangay 1993], is generality. This is apparent in the following characteristics of RhoVeR:

- **Distributed.** The system harnesses multiple interconnected processors.
- **Multiplatform.** The system functions across a range of Unix-based operating systems and hardware configurations. Currently Linux, SunOS and Solaris are supported.

- **Multiprogramming.** The system allows independant processes to execute concurrently on a single machine.

An application can select from among these features. In its full generality, RhoVeR caters for multiple processes executing on multiple machines, each with a different Unix-based operating system resident.

These features are realized in RhoVeR with a modular event-driven scheme. Each process is an instance of a module, be it of input, output, world or object type. The core of each process is an event-handling loop which accepts, processes and generates events, to and from other processes. Inter-process event-passing utilizes the Unix Socket, a sophisticated mechanism for establishing pipe-like communication between processes across a network.

Data distribution is implemented as a combination of Virtual Shared Memory (VSM) and local process cacheing. Logically, Virtual Shared Memory corresponds to the database being replicated in every process. Physically, the database is only duplicated once on every machine and processes have recourse to this data through Unix Shared Memory, a mechanism for granting processes common access to a block of memory. The VSM stores information which is of global significance, such as an object's position and orientation. Local data, such as an object's shape, is cached in the associated process, and is only accessible through a data request event. Further details on the implementation of RhoVeR appear in Appendix C.

5.2 The Virtual Sculpting Testbed

The flexibility of RhoVeR is exploited in assembling a Virtual Sculpting Testbed, the purpose of which is to experiment with Directly Manipulated Free-Form Deformation in a Virtual Environment.

A process/event structure for this testbed is detailed in figure 5.1. This reflects the stable state of the testbed and ignores the flurry of initialization events. On the input end, the system combines, in various configurations, a pair of left- and right-hand Fifth Dimension Technologies (5DT) 5thGloves and a Polhemus InsideTRAK device. The 5thGlove is

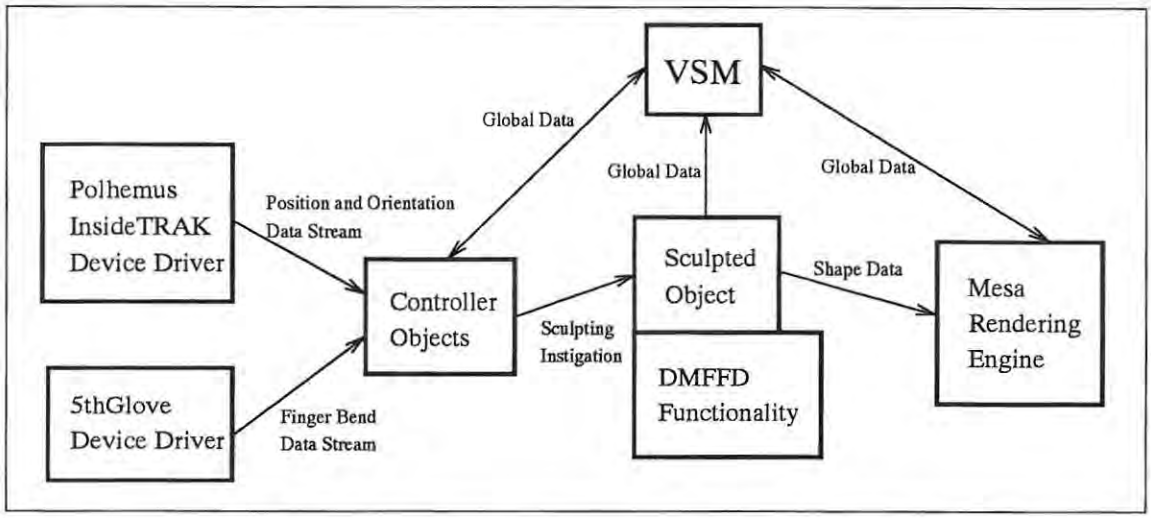

Figure 5.1: Process-Event Structure of a Virtual Sculpting Testbed

sewn from form-fitting black Lycra with fibreoptics outlining each finger (see Appendix A). Finger flexion is measured by refraction caused as the fibreoptic thread is bent. This data is transmitted to a PC Serial Port at a rate of roughly sixteen updates per second. The Polhemus InsideTRAK couples a magnetic transmitter with two sensors. Each sensor contains a set of perpendicular coils for determining its position and orientation relative to the transmitter. The device plugs into an ISA (Integrated Systems Architecture) slot on a host PC and data is placed alternately by each sensor onto the ISA bus at a combined rate of sixty updates per second. This hardware is matched by RhoVeR's InsideTRAK and 5thGlove device driver software, which pipes extracted position, orientation and finger bend data to controller objects.

The Virtual Shared Memory (VSM) serves as a central collation area for data of global significance, and it is accessible to all processes. It is from here that Controller Objects and the Mesa rendering engine extract system information, and to here that the Sculpted and Controller Objects register their ongoing changes.

Controller objects fulfil a dual function as virtual objects and control agents. A virtual hand is a typical controller object. It is a hierarchical virtual object comprising a palm and five finger-shaped solids, whose position and orientation are dictated by the device drivers and stored in Virtual Shared Memory. It is also a control agent which instigates events in response to global conditions, such as an intersection of the controller and hand object's

bounding spheres.

The Sculpted Object is a mutable solid that has recourse to DMFFD functionality and responds to events from the Controller Objects. This response may be a trivial repositioning, or a complex shape alteration. In the latter case, the following occurs: the initiating event is analyzed, a set of Direct Manipulation vectors is constructed and fed to the DMFFD subsystem, the prescribed changes in locally cached vertices are effected and the shape-change counter in the VSM is incremented.

The Mesa three-dimensional graphics library is a platform independent OpenGL lookalike. It emulates the command syntax and state-machine of OpenGL, Silicon Graphic's Application Programming Interface (API). The Rendering Engine for this testbed utilizes Mesa for display, under the Linux, SunOS and Solaris operating systems. Complete shape, colour, position and orientation information for every object in the testbed is stored in this process, and is updated from the VSM or Sculpted Object cache as required.

The sculpting applications, which fill the remainder of this chapter, fit seamlessly within the framework of this Virtual Sculpting Testbed.

5.3 Interactive Surface Sketching

Surface Reconstruction strives to form a computer replica of a physical object from sampled information. At its most general, this means crafting a shape of arbitrary topology from an unorganized mass of three-dimensional points. This is an extremely exacting operation which can be simplified by exploiting the structure inherent in most sampling processes. In this regard, three classes of sampling have been identified [Hoppe *et al* 1992]:

- **Range Data.** This is typically a rectangular grid of depth values (from sensor to solid) generated by the regular horizontal and vertical sweep of a laser range finder. To build a complete model, either the solid must be spun, or the sensor successively relocated, so that the data can be integrated from varying viewpoints.

- **Contours.** Here, a stack of cross-sections or contours is accumulated slice by slice. This procedure deals poorly with protuberances orthogonal to the scanning axis and complex branching structures. Nevertheless, many medical scanning techniques fall in this category.

- **Interactive Surface Sketching.** A model is gradually evolved by recording the path of a tracker traced across the surface of the object. 3-DRAW [Sachs *et al* 1991] is a progenitor of surface sketching and it produces three-dimensional free-form curves matched to the motion of a stylus with Polhemus tracker attached.

DMFFD offers an elegant solution to this last problem. At a physical level, the user grasps in one hand the real-world object to which a Polhemus tracker (designated as the *reference*) is taped. The other hand is used to slide the second tracker (referred to as the *tracer*) over the object's surface. The inclusion of a *reference* tracker means that the object can be turned and moved freely during sketching as long as both trackers remain in contact. On a logical plane, an enclosing sphere is progressively deformed with each successive *tracer* position, while previous points are simultaneously pinned in place.

There are three restrictions imposed on this sketching:

1. **Ordered Sampling.** The stream of tracker positions must be picked up and dealt with in sequence.

2. **No Holes.** The real-world object being sketched must have no holes that pass entirely through the object. Otherwise simple solids, such as tori and coffee cups, are thus forbidden.

3. **Smooth Tracing.** Tracker movement must be gradual and controlled, with no abrupt changes in either speed or direction.

With these properties in mind, interactive DMFFD-based surface sketching proceeds in three stages:

1. As a preliminary, a bounding sphere, which entirely surrounds the object, is fashioned (see figure 5.2). This is accomplished by waving the *tracer* in broad circles around

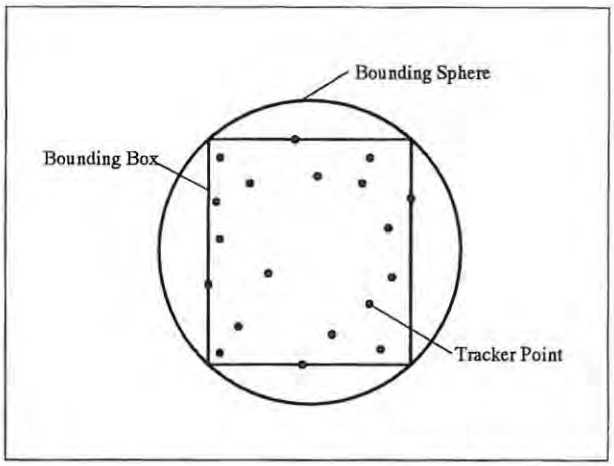

Figure 5.2: Creating a Bounding Sphere

the physical object. A cloud of points is churned out and stored relative to the *reference* tracker. A cube, and subsequently a sphere, which enfold this cloud, are then generated. The bounding sphere is an independent virtual sculpted object and a rough first-pass analogue of the physical object.

2. Next, the sculpted object is contained in a lattice grid and the *tracer* placed against the physical object. Then the sphere is pressed in by DMFFD towards the *reference* and *tracer* positions. This completes the setup steps and the pivotal sketching iteration can now be outlined.

3. As each successive *tracer* location is received it is processed as shown in figure 5.3:
[A] It is ignored if it is too close to any of the previously collected points. This separation allows accidental retracing of portions of the solid and prevents overconstraint.
[B] A DM point (I) on the surface of the sculpted object is determined. This procedure relies on the current *tracer* (T_0) and two previous *tracer* (T_1, T_2) positions as well as the distance from T_0 to T_1 denoted by D. A fourth point (P) is placed co-linear with T_1 and T_2 and a distance D beyond T_1. Then I is the closest point to P on the surface. The associated DM vector is from this intersection I to T_0.
[C] Next a set of DM points and associated vectors are collated. The first element in these sets are the point I and vector $I \rightarrow T_0$. After this, all those previous DM points lying within the same or neighbouring lattice cells as I are included and pinned into place with null DM vectors.
[D] Finally, the sculpted object undergoes DMFFD and a better fit to its mirroring

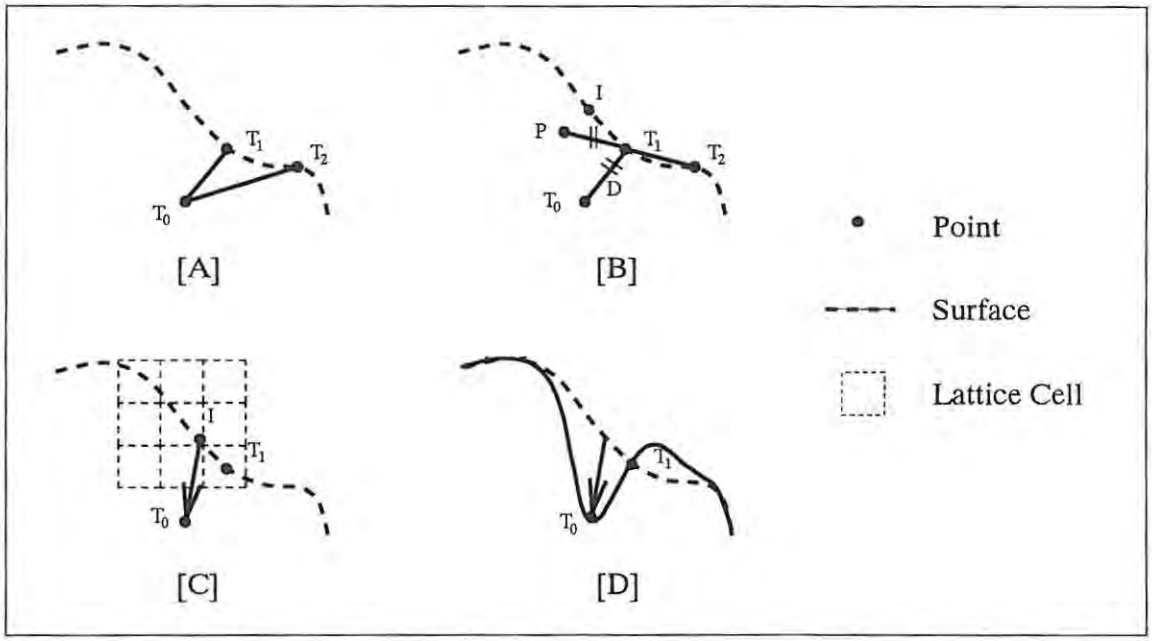

Figure 5.3: Surface Sketching Loop [A] Distance Testing, [B] Determining new DM point and vector, [C] Building Pinning Points, [D] Direct Manipulation

object in the real world is obtained.

5.4 Glove-based Moulding

The intention of Glove-based moulding is to enrich the clay-sculpting analogy by controlling interaction and deformation with a dataglove. From the user's viewpoint the twisting, translation and flexing of the dataglove are mirrored by a virtual hand, which kneads and manipulates a virtual lump of clay. Dataglove directed DMFFD has been suggested [Hsu *et al* 1992], but neither specified nor implemented until now.

The glove-based moulding procedure takes as its input two successive snapshots of the position, orientation and finger flexion of a dataglove. These pre- and post-images of the glove are then processed with reference to the sculpted object, and a set of Direct Manipulation points and vectors are generated. For DMFFD purposes the virtual hand is defined by a set of evenly distributed *controller points*. An individual moulding operation proceeds in three steps (as per figure 5.4):

1. Two complete sets of three-dimensional *controller point* positions are extracted from the pre- and post-images of the glove.
2. The corresponding *controller points* in each hand image are joined by a *controller segment.*
3. Each *controller segment* is enclosed by a parallelpiped volume, which is then intersected with the sculpted object's surface to yield a collection of Direct Manipulation points and vectors.

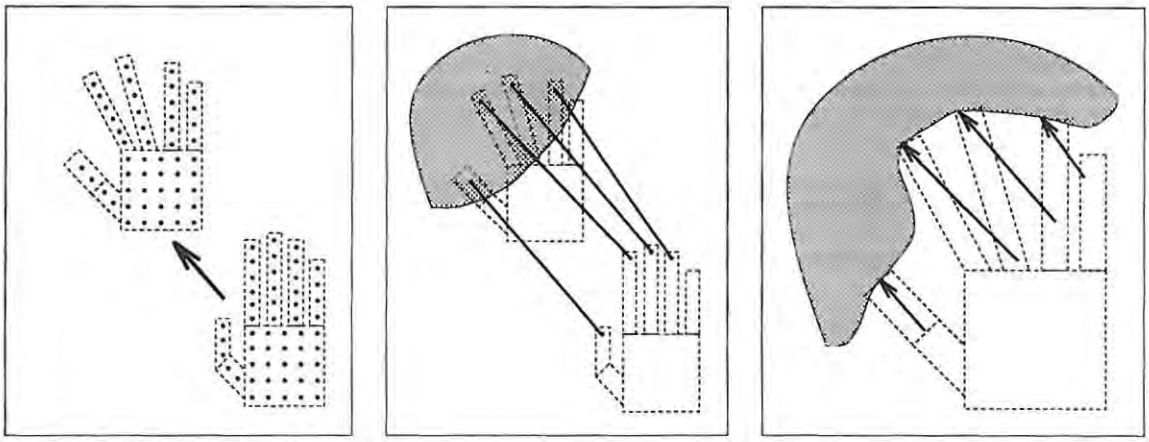

[A] [B] [C]

Figure 5.4: Glove-based Moulding: [A] Pre- and Post-Images of the Virtual Hand with *Controller Points*, [B] *controller segments* joining selected *controller points*, [C] Direct Manipulation vectors and Sculpted Object deformation.

There are several additional points worth noting about this procedure:

- There is some processing to eliminate those occluded *controller segments* which lie in the shadow of others, and some DM vectors are weeded out to prevent overconstraint.
- The lattice that accompanies this Direct Manipulation is linked to the initial spacing of *controller points*. This means that by scaling the hand in proportion to the sculpted object, the scope and effect of deformations can be varied.
- Changes in the data glove must not be overly rapid relative to the data capture rate, otherwise some of the intricacies of its motion, and hence deformation, will be lost.

Appendix A provides colour plates which illustrate this application.

5.5 Concluding Remarks

This chapter has tested the utility of DMFFD in a Virtual Environment with two representative applications: interactive surface sketching and glove-based moulding. These applications have successfully abstracted away from specifying Directly Manipulated vectors, to a more intuitive interface.

Chapter 6

Conclusion

6.1 Conclusions

A Virtual Sculpting system has been developed to address the task of Free-Form Solid Modelling. The disparate elements of a Polygon-Mesh representation, a Directly Manipulated Free-Form Deformation sculpting tool, and a Virtual Environment have been drawn into a cohesive whole under the mantle of a clay-sculpting metaphor. The principles of intuitivity, versatility and, especially interactivity have been re-examined at every stage of development and several novel enhancements considered.

Measures to reinforce the clay-sculpting analogy have had concomitant benefits for intuitivity. Firstly, the Quadratic or Cubic Uniform Rational B-Spline foundations of DMFFD guarantee smoothly moulded surfaces (of C^1 or C^2 continuity respectively). There was a danger that the approximation inherent in the Polygon-Mesh representation combined with the constant flexing induced by DMFFD would compromise this smoothness, but this has been solved by the mesh refinement and decimation schemes of Chapter 4. Secondly, the ease with which deformations are specified and controlled has been improved. The original Free-Form Deformations [Sederberg and Parry 1986] were instigated by repositioning control vertices in a lattice. Later Direct Manipulation extensions [Hsu *et al* 1992] allayed this indirection and obfuscation by providing a mechanism for dragging points on a solid's surface directly. In this work, the directly manipulated points are, in turn, subsumed into

Virtual Controllers such as a "hand", "suction-cup" or "surface sketcher". Also, A Virtual Environment is an intrinsically three-dimensional interface. This alone contributes considerable intuitivity. Finally, this work raised and resolved the issue of self-intersection, an occasional counter-intuitive side-effect of DMFFD. The circumstances under which it occurred were identified and measures for avoiding it were prescribed.

One of the attractive features of Directly Manipulated Free-Form Deformation is its versatility. The scope of DMFFD can be tuned between highly localised and completely global deformations; it is point-based and thus largely representation independent, and has a wide range of potential applications.

Free-Form Deformation is notoriously inefficient, and this is exacerbated by the Direct Manipulation extensions. Considerable attention has been paid to efficiency issues over the course of this thesis, and it is here that the main contribution lies. In Chapter 2, three simple but effective alterations of Free-Form Deformation were proposed. In Chapter 3, the core computation of Direct Manipulation, a least squares solution to an underdetermined system of linear equations was analyzed. A method based on a Choleski Factorization of Normal Equations was found to provide a fourfold increase in speed over the original approach [Hsu *et al* 1992]. A unique modification of this method, which made it both considerably more compact and independent of the spread of Direct Manipulation across lattice cells, was then effected. These enhancements combine to make a qualitative difference in the viability of DMFFD as an interactive sculpting tool.

6.2 Future Work

At each layer of the Free-Form Modelling system developed in this thesis, there are opportunities for additional exploration, experimentation and enhancement. These directions for future research span the Foundations (Chapter 2), Topology (Chapter 4), and Applications (Chapter 5) sections of this thesis.

6.2.1 Replacing the Underlying Splines

This work is founded on the Quadratic and Cubic Uniform Rational B-Splines because of their continuity, local control, convex hull, and above all efficiency properties, but the substitution of Non-Uniform Rational B-Splines (NURBS) or β-Splines might be advantageous. NURBS would allow simultaneous intricate convolution and widespread gradation, depending on how tightly or loosely packed the NURBS lattice cells were in a particular region. For β-Splines, the apparent consistency of the sculpted solid could be varied by tuning the bias and tension parameters. The difficulty would be incorporating these splines into the mathematics of DMFFD. Another challenge would be to substitute splines seamlessly so that the increased versatility does not overwhelm either interactivity or the illusion of sculpting.

6.2.2 Complex Lattices

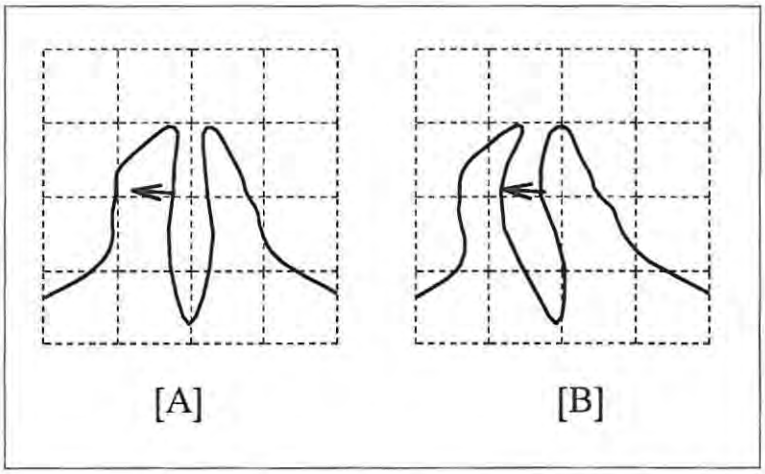

Figure 6.1: Undesirable Volume-based effects. [A] Pre-Deformation, [B] Post-Deformation.

The FFD lattice in this work is severely restricted. Lattice cells are identical parallelpipeds fixed in line with the co-ordinate axes. In general, these restrictions augment intuitivity and do not in any way curtail the range of possible deformations. However, there is a counter-intuitive side-effect that stems from the volume-oriented nature of FFD (see figure 6.1). This can only be circumvented by varying the size [Lamousin and Waggenspack 1994] or

shape [Coquillart 1990] of cells within the lattice, but again incorporating these into Direct Manipulation is far from trivial. A lattice that is tailored to fit an object will retain desirable and prevent undesirable volume warping, but this intuitivity can only be gained at the expense of interactivity.

6.2.3 Analysis of Self-Intersection

The study of self-intersection in Chapter 4 was informal and heuristic. The problem would benefit from formal and mathematically rigorous analysis. The product of this research would be either a classification that precisely separated valid and invalid Direct Manipulation, or, preferably, a modification of the DMFFD mechanism, to inhibit self-intersection without disallowing particular Direct Manipulations.

6.2.4 Piercing Holes in the Solid

A solid is normally topologically invariant under DMFFD. Thus, no vertices, edges, faces or holes are ever introduced by DMFFD itself. This is why the applications of Chapter 5 are limited to cohesive solids, which have no holes and can be bulged and expanded into a topologically equivalent sphere. An exacting but natural extension of the previous section would be to replace self-intersection with hole creation, thereby mimicking the perforation of clay and expanding the diversity of possible shapes.

6.2.5 Further Applications

The Interactive Surface Sketching and Glove-Based Moulding of Chapter 5 are the forerunners of an abundance of potential DMFFD applications:

1. **Two-Handed Glove-Based Moulding.** Left and right-handed datagloves can be used in tandem to manipulate a solid. There is an increase in possible self-intersections, but this is more than counterbalanced by the enriched precision, power and ease-of-use engendered by this approach.

2. **Extrusion.** Up until now, surface points have generally been pushed inwards rather than dragged outwards. An extrusion mode could be implemented, perhaps with a "sticky fingers" or "suction-cup" paradigm.

3. **Imprinting.** A two-dimensional figure, such as a letter, numeral or symbol can be defined by a linked sequence of *stencil-points* set in a plane. This plane is then pressed into a solid and direct manipulation vectors extracted from the motion of the *stencil-points* intersecting with the solid's surface. The associated deformation will stamp or imprint the original figure into the solid.

4. **Sculpted Set Operations.** The previous technique may be extrapolated to imprinting or merging a three-dimensional *actor* with a solid in a fashion analogous to conventional set operations, except that the result is tapered rather than sliced and suggestive of an impenetrable *actor* interacting with a malleable object. The difficulty here is determining the frequency and distribution of *stencil-points* on the boundary of the *actor*.

Appendix A

Colour Plates

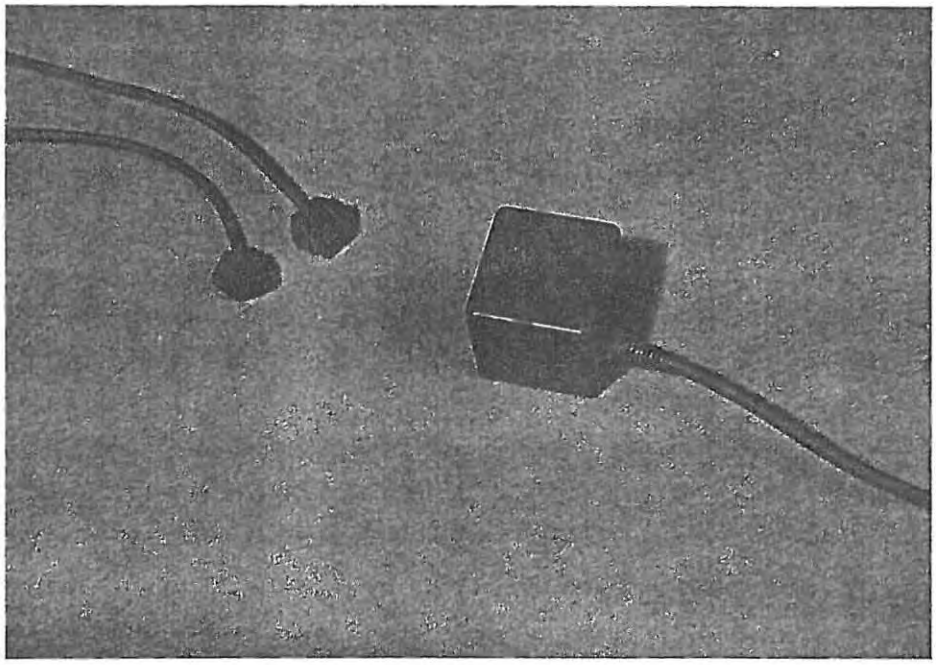

Figure A.1: The Polhemus InsideTRAK.

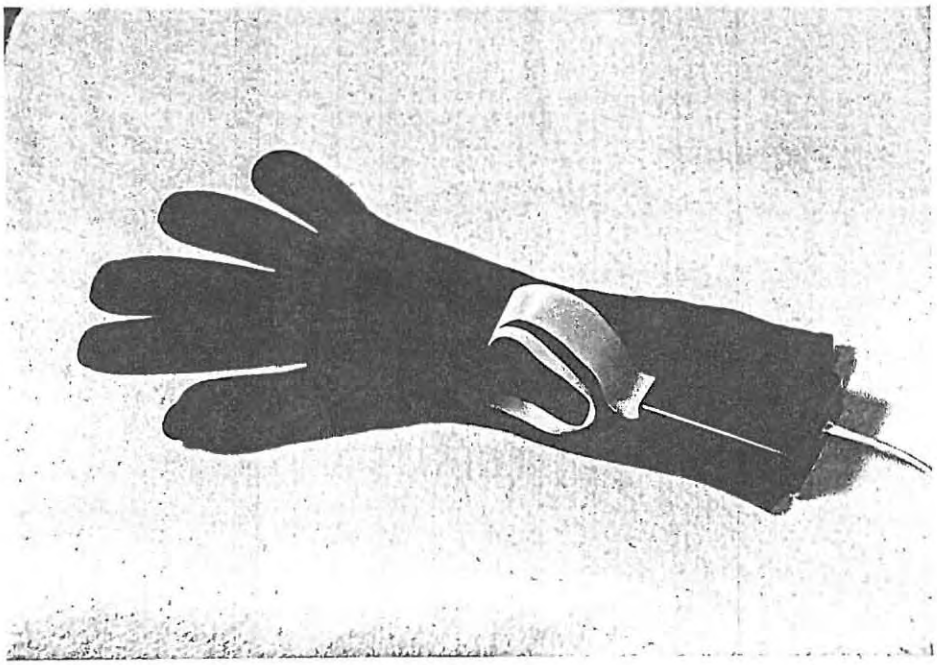

Figure A.2: The Fifth Dimension Technologies 5thGlove.

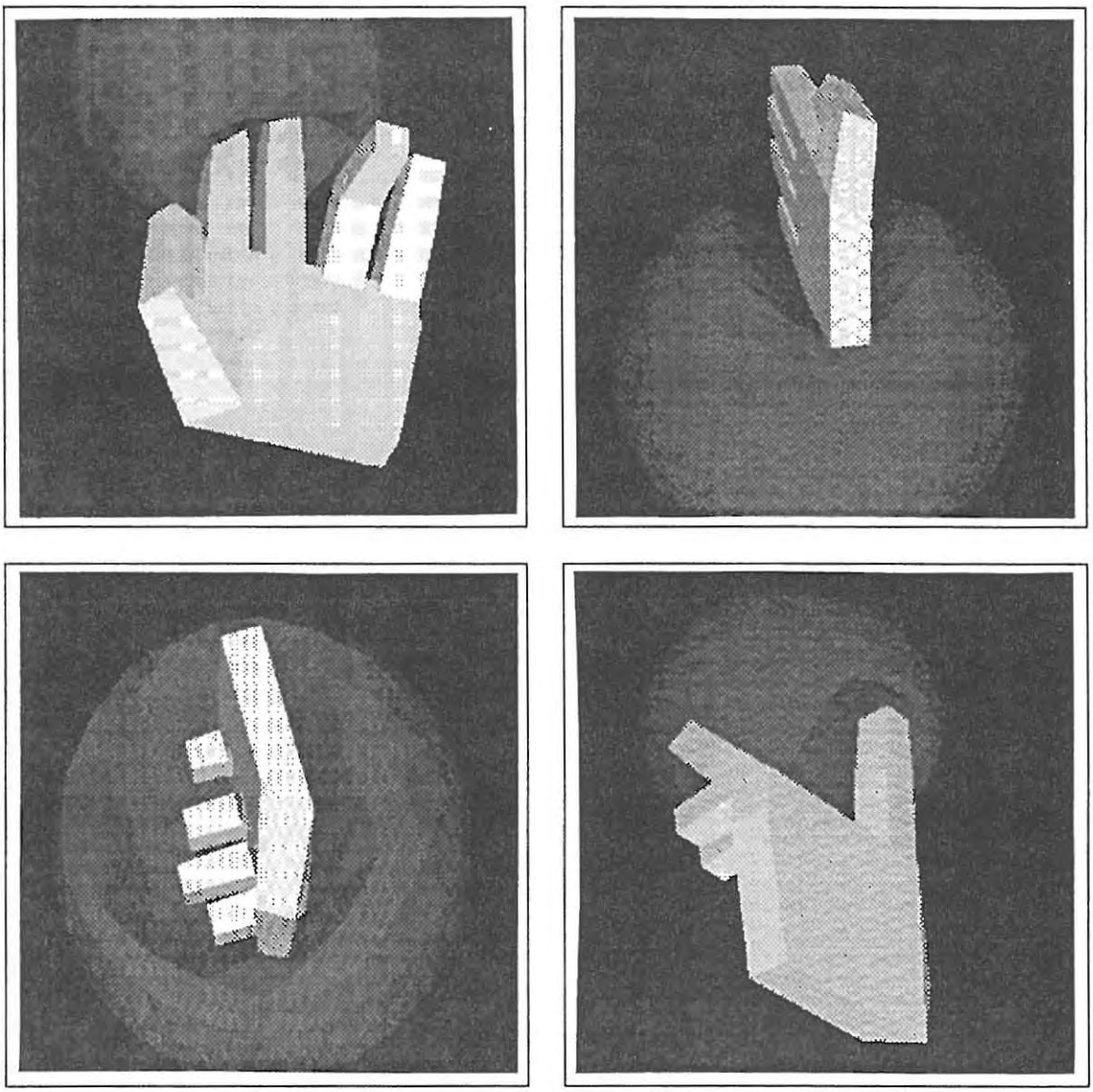

Figure A.3: Glove-based Moulding.

Appendix B

Directly Manipulated Free-Form Deformation Program Extracts

```
/* file: ffd.h
   author: James Gain
   project: Virtual Sculpting
   notes: An enhanced implementation of Free-Form Deformation (Sederburg and Parry)
               with Direct Manipulation Extensions (Hsu).
*/

#include "vector.h"
#include "matrix.h"

#define MAXLATDIM 50
#define LATDIMCUBED 125000
#define MAX3LATDIM 150
#define DEGREE 3    // 2 implies C1 and 3 implies C2

/* LATTICE: An initially uniform subdivision of 3-space into URBS cells.
   lat_origin:  The origin of the lattice cell space.
   grid_origin: The origin of the lattice grid space.
   span:        The extent of the lattice along the x, y and z axes.
   l, m, n:     The number of deformable and influenced cells
                along the x, y, z axes.
   grid:        A 3-dimensional matrix which holds the control point
                positions of the lattice.
   cell:        length of an individual cell along the x, y and z axes.
   delpoints:   An index of boolean entries corresponding to grid and
                flagging changes in control points from their initial
                uniform state
   delcells:    An index of boolean entries flagging whether a point
```

```
        located in the flagged cell will be moved under FFD */

class lattice
{ point lat_origin, grid_origin;
  vector span, cell;
  int l,m,n;
  double * grid[MAXLATDIM];
  char delpoints[MAXLATDIM][MAXLATDIM][MAXLATDIM];
  char delcells[MAXLATDIM][MAXLATDIM][MAXLATDIM];
  matrix mat[8];
  basismtx B;

  /* locatepnt: locate a point in the FFD lattice
                given: pnt = an undeformed 3d point
                return: i,j,k = the indices of pnt's cell
                        loc = the local co-ordinates of pnt in that cell
                error: 0 if the point is outside the scope of the ffd lattice
                       2 if the point is in an influenced cell
                       1 if the point is in a deformable cell  */
  int lattice::locatepnt(point & pnt,int & i,int & j,int & k, point & loc);

  /* get: retrieve a grid point stored as an increment
          given:  u, v, w = index of control point position in grid
          return: pnt = the point at this position  */
  inline void get(int u, int v, int w, point & pnt)
  { int vconst, wconst;

    vconst = v * MAX3LATDIM;
    wconst = w * 3;
    pnt.x = (grid[u])[vconst + wconst];
    pnt.y = (grid[u])[vconst + wconst+1];
    pnt.z = (grid[u])[vconst + wconst+2];
  }

  /* incr: increase a grid points value
           given: u, v, w = index of control point position in grid
                  pnt = increment value */
  inline void incr(int u, int v, int w, point pnt)
  { int vconst, wconst;

    vconst = v * MAX3LATDIM;
    wconst = w * 3;
    (grid[u])[vconst + wconst] += pnt.x;
    (grid[u])[vconst + wconst+1] += pnt.y;
    (grid[u])[vconst + wconst+2] += pnt.z;
  }
```

```
  /* set: place a grid points value
          given u, v, w = index of control point position in grid
                pnt = new grid point */
  inline void set(int u, int v, int w, point pnt)
  { int vconst, wconst;

    vconst = v * MAX3LATDIM;
    wconst = w * 3;
    (grid[u])[vconst + wconst] = pnt.x;
    (grid[u])[vconst + wconst+1] = pnt.y;
    (grid[u])[vconst + wconst+2] = pnt.z;
  }

  public:

    /* default constructor: allocate memory for lattice structure and
                            initialize variables */
    lattice();

    /* reset: initialize the lattice
              given: (parameters for the deformable region)
                     base = the lattice origin;
                     dx, dy, dz = the range of the lattice along x, y and z axes;
                     i, j, k = number cells along x, y, z axes */
    void lattice::reset(point base,double dx,double dy,double dz,
                    int i,int j,int k);

    /* clear: re-establish a base-state lattice */
    void lattice::clear();

    /* multimanip: multiple point direct manipulation of a FFD lattice.
                   given: sizeq = number of DM points
                          q = coords of DM points
                          deltaq = DM motion vectors
                   return: alter the corresponding lattice grid points */
    void lattice::multimanip(int sizeq, point * q, vector * deltaq);

    /* applyFFD: Apply the FFD lattice to a single point in 3D space.
                 given: objpoint = the point to be deformed
                 error: 1 if objpoint is altered
                        0 if it is not */
    int lattice::applyFFD (point & objpoint);

};
```

```
/* file: ffd.c
   author: James Gain
   project: Virtual Sculpting
   notes: An enhanced implementation of Free-Form Deformation (Sederburg and Parry)
          with Direct Manipulation Extensions (Hsu).
*/

#include <stdlib.h>
#include <math.h>
#include <string.h>

#include "urbs.h"
#include "ffd.h"

/* locatepnt */
int lattice::locatepnt(point & pnt,int & i,int & j,int & k, point & loc)
{ int retval;
  vector PminusOrigin, scale;

  /* stage1: locate point as scaling of span vector. */
  PminusOrigin = pnt - lat_origin;
  scale = PminusOrigin / span;

  /* stage2: if scale is < 0 > 1 return 0 otherwise locate it in local
             cell (i,j,k) and assign new co-ordinates (loc) */
  if ((scale.i < 1.0)&&(scale.i >= 0.0)&&(scale.j < 1.0)&&(scale.j >= 0.0)
      &&(scale.k < 1.0)&&(scale.k >= 0.0))
  { i = (int) (scale.i * (double) l);
    j = (int) (scale.j * (double) m);
    k = (int) (scale.k * (double) n);

    loc.x = ((double) l * scale.i) - (double) i;
    loc.y = ((double) m * scale.j) - (double) j;
    loc.z = ((double) n * scale.k) - (double) k;

    if ((i < DEGREE) || (i >= l-DEGREE) || (j < DEGREE) || (j >= m-DEGREE)
        || (k < DEGREE) || (k >= n-DEGREE))
      // influenced zone cells
      retval = 2;
    else
      // deformable zone cells
      retval = 1;
  }
  else
    retval = 0;
  return retval;
}
```

```
/* default constructor */
lattice::lattice()
{ register int create;
  long tmpsize;

  l = 0; m = 0; n = 0;

  for(create = 0; create < MAXLATDIM; create++)
  { tmpsize = (MAX3LATDIM * MAXLATDIM) * sizeof(double);
    grid[create] = (double *) malloc(tmpsize);
    if(grid[create] == NULL)
      printf("ERR (ffd.lattice) ==> unable to allocate lattice grid\n");
  }

  for(create = 0; create < 6; create++)
    mat[create].create(64, 64);
  B.create(64);
}

/* reset */
void lattice::reset(point base,double dx,double dy,double dz,
                    int i,int j,int k)
{ register int a, b, c;

  // adjustment for influenced cells
  span.i = dx;
  span.j = dy;
  span.k = dz;
  l = i + DEGREE * 2;
  m = j + DEGREE * 2;
  n = k + DEGREE * 2;

  if(((l+1)>MAXLATDIM) || ((m+1)>MAXLATDIM) || ((n+1) > MAXLATDIM))
     fprintf(stderr,"ERR (ffd.reset) ==> lattice dimensions exceed
                     limits\n");

  cell.i = span.i / ((double) i);
  cell.j = span.j / ((double) j);
  cell.k = span.k / ((double) k);

  lat_origin = base + (cell * ((double) DEGREE * -1.0));
  #if (DEGREE == 2)
  grid_origin = base + (cell * -2.5);
  #else
  grid_origin = base + (cell * -4.0);
  #endif
```

```
  // adjust for influenced cells
  span.i = cell.i * (double) l;
  span.j = cell.j * (double) m;
  span.k = cell.k * (double) n;

  // reset delpoints and delcells
  memset(delpoints, 0, LATDIMCUBED);
  memset(delcells, 0, LATDIMCUBED);
}

/* clear */
void lattice::clear()
{ memset(delpoints, 0, LATDIMCUBED);
  memset(delcells, 0, LATDIMCUBED);
}

/* multimanip */
void lattice::multimanip(int sizeq, point * q, vector * deltaq)
{ int bfill, inside, i, j, k;
  double basis;
  double basis_s[DEGREE+1], basis_t[DEGREE+1], basis_u[DEGREE+1];
  point delta, coord;
  int m, n, dim;
  double value, y[64];
  index curr, xindex, yindex;
  register int xi, xj, xk, a, b, c, yi, yj, yk, row = 0, col = 0;

  if(sizeq > 0)
  {

  // create basis matrix B
  for(bfill = 0; bfill < sizeq; bfill++)
  { inside = this->locatepnt(q[bfill], i,j,k,coord);

    if(inside == 1)
    { for(a = i-DEGREE; a <= i+DEGREE; a++)
        for(b = j-DEGREE; b <= j+DEGREE; b++)
          for(c = k-DEGREE; c <= k+DEGREE; c++)
            delcells[a][b][c] = 1;

      mat[5].put(row, 0, deltaq[bfill].i);    // copy deltaq
      mat[5].put(row, 1, deltaq[bfill].j);
      mat[5].put(row, 2, deltaq[bfill].k);

      #if (DEGREE == 2)
        quad_basisarray(coord.x, basis_s);
        quad_basisarray(coord.y, basis_t);
        quad_basisarray(coord.z, basis_u);
      #else
```

```
      cubic_basisarray(coord.x, basis_s);
      cubic_basisarray(coord.y, basis_t);
      cubic_basisarray(coord.z, basis_u);
    #endif

    B.putindex(row, i, j, k);
    for(a = 0; a <= DEGREE; a++)
      for(b = 0; b <= DEGREE ; b++)
        for(c = 0; c <= DEGREE; c++)
        { basis = basis_s[a] * basis_t[b] * basis_u[c];
          B.putval(row, a, b, c, basis);
        }
    row++;
  }
}

B.row = row;
mat[5].row = row;   mat[5].col = 3;


// form normal equations from basis matrix B
m = B.row;
mat[1].row = m; mat[1].col = m;
for(row = 0; row < m; row++)
{  for(col = 0; col <= row; col++)
  {
    xindex = B.getindex(row);
    yindex = B.getindex(col);

    switch(yindex.i - xindex.i)
    { case 0: xi = 0; yi = 0; i = DEGREE+1; break;
      case 1: xi = 1; yi = 0; i = DEGREE; break;
      case 2: xi = 2; yi = 0; i = DEGREE-1; break;
      case 3: xi = 3; yi = 0; i = DEGREE-2; break;
      case -1: xi = 0; yi = 1; i = DEGREE; break;
      case -2: xi = 0; yi = 2; i = DEGREE-1; break;
      case -3: xi = 0; yi = 3; i = DEGREE-2; break;
      default: i = 0; break;
    }
    switch(yindex.j - xindex.j)
    { case 0: xj = 0; yj = 0; j = DEGREE+1; break;
      case 1: xj = 1; yj = 0; j = DEGREE; break;
      case 2: xj = 2; yj = 0; j = DEGREE-1; break;
      case 3: xj = 3; yj = 0; j = DEGREE-2; break;
      case -1: xj = 0; yj = 1; j = DEGREE; break;
      case -2: xj = 0; yj = 2; j = DEGREE-1; break;
      case -3: xj = 0; yj = 3; j = DEGREE-2; break;
      default: j = 0; break;
    }
    switch(yindex.k - xindex.k)
```

```
    { case 0: xk = 0; yk = 0; k = DEGREE+1; break;
      case 1: xk = 1; yk = 0; k = DEGREE; break;
      case 2: xk = 2; yk = 0; k = DEGREE-1; break;
      case 3: xk = 3; yk = 0; k = DEGREE-2; break;
      case -1: xk = 0; yk = 1; k = DEGREE; break;
      case -2: xk = 0; yk = 2; k = DEGREE-1; break;
      case -3: xk = 0; yk = 3; k = DEGREE-2; break;
      default: k = 0; break;
    }

    value = 0.0;
    for(a = 0; a < i; a++)
      for(b = 0; b < j; b++)
        for(c = 0; c < k; c++)
          value += B.getval(row, a+xi, b+xj, c+xk)
                   * B.getval(col, a+yi, b+yj, c+yk);
    mat[1].put(row,col,value);
  }
}


// by symmetry upper triangle mirrors lower
for(j = 1; j < m; j++)
  for(i = 0; i < j; i++)
    mat[1].put(i, j, mat[1].get(j, i));

// Choleski Factorization
value = sqrt(mat[1].get(0,0));
mat[2].put(0,0, value);
for(j = 1; j < m; j++)
  mat[2].put(j, 0, mat[1].get(j, 0) / value);
for(i = 1; i < (m-1); i++)
{ value = 0.0;
  for(k = 0; k < i; k++)
    value += mat[2].get(i, k) * mat[2].get(i, k);
  mat[2].put(i, i, sqrt(mat[1].get(i, i) - value));
  for(j = i+1; j < m; j++)
  { value = 0.0;
    for(k = 0; k < i; k++)
      value += mat[2].get(j, k) * mat[2].get(i, k);
    mat[2].put(j, i, (mat[1].get(j, i) - value)/mat[2].get(i, i));
  }
}

value = 0.0;
for(k = 0; k < (m-1); k++)
  value += mat[2].get(m-1, k) * mat[2].get(m-1, k);
mat[2].put(m-1, m-1, sqrt(mat[1].get(m-1, m-1) - value));

for(dim = 0; dim < 3; dim++)
```

```
  { y[0] = mat[5].get(0,dim)/mat[2].get(0,0);
    for(i = 1; i < m; i++)
    { value = 0.0;
      for(j = 0; j < i; j++)
        value += mat[2].get(i, j) * y[j];
      y[i] = (mat[5].get(i,dim) - value)/mat[2].get(i, i);
    }
    mat[3].put(m-1, dim, y[m-1] / mat[2].get(m-1, m-1));
    for(i = (m-2); i >= 0; i--)
    { value = 0.0;
      for(j = i+1; j < m; j++)
        value += mat[2].get(j, i) * mat[3].get(j, dim);
      mat[3].put(i, dim, (y[i] - value)/mat[2].get(i, i));
    }
  }

  // mult mat[3] by Btranspose and alter lattice
  for(row = 0; row < m; row++)
  { curr = B.getindex(row); xi = curr.i; xj = curr.j; xk = curr.k;
    for(a = 0; a <= DEGREE; a++)
      for(b = 0; b <= DEGREE; b++)
        for(c = 0; c <= DEGREE; c++)
        {
          value = B.getval(row, a, b, c);
          delta.x = value * mat[3].get(row, 0);
          delta.y = value * mat[3].get(row, 1);
          delta.z = value * mat[3].get(row, 2);

          // add directly to lattice
          if(delpoints[xi+a][xj+b][xk+c])
            this->incr(xi+a, xj+b, xk+c, delta);
          else
          { delpoints[xi+a][xj+b][xk+c] = 1;
            this->set(xi+a, xj+b, xk+c, delta);
          }
        }

    }
  }
}
```

```
/* applyFFD */
int lattice::applyFFD (point & objpoint)
{ double basisX[DEGREE+1], basisY[DEGREE+1], basisZ[DEGREE+1],
         accumx, accumy, accumz, weight, tweenweight;
  register int a, b, c, i, j, k;
  point pnt, coord;
  int u, v, w;

  if (this->locatepnt(objpoint, u, v, w, coord))
  { i = u; j = v; k = w;
    if(delcells[i][j][k])
    {
      #if (DEGREE == 2)
        quad_basisarray(coord.x, basisX);
        quad_basisarray(coord.y, basisY);
        quad_basisarray(coord.z, basisZ);
      #else
        cubic_basisarray(coord.x, basisX);
        cubic_basisarray(coord.y, basisY);
        cubic_basisarray(coord.z, basisZ);
      #endif

      accumx = 0.0;
      accumy = 0.0;
      accumz = 0.0;

      for(a = 0; a <= DEGREE; a++)
        for(b = 0; b <= DEGREE; b++)
        { tweenweight = basisX[a] * basisY[b];
          for(c = 0; c <= DEGREE; c++)
          { weight = tweenweight * basisZ[c];
            if(delpoints[i+a][j+b][k+c])
            { // grab modified grid point from memory
              this->get(i+a,j+b,k+c, pnt);
              accumx += pnt.x * weight;
              accumy += pnt.y * weight;
              accumz += pnt.z * weight;
            }
          }
        }
      objpoint.x += accumx;
      objpoint.y += accumy;
      objpoint.z += accumz;
      return 1;
    }
  }
  return 0;
}
```

```
/* file: matrix.h
     author: James Gain
     project: Virtual Sculpting
     notes: standard matrix and sparse basis matrix functions
*/

#include <stdio.h>

#define MAXMATDIM 70

class index
      { public:
          int i, j, k;

          /* index: default constructor */
          index()
          { i = 0;
            j = 0;
            k = 0;
          }

      };

struct cell
      { double block[4][4][4];
      };

class basismtx
      { cell * mtx[MAXMATDIM];
        index latloc[MAXMATDIM];

        public:
          int row, col;

          /* create: allocate and initialize a basis matrix */
          void create(int down);

          /* get: returns the value (at getrow, i, j, k) or index (getrow)
          of the matrix */
          inline double getval(int getrow, int i, int j, int k)
          {
             return (* mtx[getrow]).block[i][j][k];
          }

          inline index getindex(int getrow)
          {
            return latloc[getrow];
          }
```

```
        /* put: inserts a value or index  at position (putrow)
        of the matrix */
        inline void putval(int putrow, int i, int j, int k,  double val)
        {
          (* mtx[putrow]).block[i][j][k] = val;
        }

        inline void putindex(int putrow, int li, int lj, int lk)
        {
          latloc[putrow].i = li;
          latloc[putrow].j = lj;
          latloc[putrow].k = lk;
        }
    };

class matrix
    { public:
        int row, col;
        double * mtx[MAXMATDIM];

        /* create: allocate and initialize a matrix */
        void create(int down,int across);

        /* get: returns the value at position (getrow, getcol) of the matrix */
        inline double get(int getrow, int getcol)
        {
           return ((mtx[getrow])[getcol]);
        }

        /* put: inserts a value at position (putrow, putcol) of the matrix */
        inline void put(int putrow, int putcol, double val)
        {
          ((mtx[putrow])[putcol]) = val;
        }

    };
```

```
/* file: vector.h
     author: James Gain
     project: Virtual Sculpting
     notes: Basic vector arithmetic library.
*/

class point
      { public:

          double x,y,z;

          /* point: default constructor */
          point();

      };

class vector
      { public:
          double i, j, k;

          /* vector: default constructor */
          vector();

          /* (*) scale: scale the vector by a scalar factor c */
          friend vector operator *(vector v, double c);

          /* (/) divide: divide the first vector by the second */
          friend vector operator /(vector a, vector b);

          /* (-) difference of points: create a vector from point P to point Q (Q-P) */
          friend vector operator -(point p, point q);

          /* (+) pnt plus vec: find the point at the head of a vector which
                                is placed with its tail at p */
          friend point operator +(point p, vector v);
      };
```

```
/* file: urbs.h
   author: James Gain
   project: Virtual Sculpting
   notes: A library for Uniform Rational Basis Spline (URBS) support.
*/

/* cubic_basisarray: Return an array containing all the spans (-3,-2,-1,0) of a
   cubic B-Spline associated with u. */
void cubic_basisarray(double u, double * array);

/* quad_basisarray: Return an array containing all the spans (-2,-1,0) of a
     quadratic B-Spline associated with u. */
void quad_basisarray(double u, double * array);
```

```
/* file: urbs.c
   author: James Gain
   project: Virtual Sculpting
   notes: A library for Uniform Rational Basis Spline (URBS) support.
*/

#include "urbs.h"

/* cubic_basisarray */
void cubic_basisarray(double u, double * array)
{ double usquared, ucubed, u3, usquared3, ucubed3;

  usquared = u * u;
  ucubed = usquared * u;
  u3 = 3.0 * u;
  usquared3 = 3.0 * usquared;
  ucubed3 = 3.0 * ucubed;
  array[3] = (ucubed/6.0);
  array[2] = ((1.0+(u3)+(usquared3)-(ucubed3))/6.0);
  array[1] = ((4.0-(6*usquared)+(ucubed3))/6.0);
  array[0] = ((1.0-(u3)+(usquared3)-ucubed)/6.0);
}

/* quad_basisarray */
void quad_basisarray(double u, double * array)
{ double usquared, usquaredhalf;

  usquared = u * u;
  usquaredhalf = 0.5 * usquared;
  array[2] = usquaredhalf;
  array[1] = 0.5 + u - usquared;
  array[0] = 0.5 - u + usquaredhalf;
}
```

Appendix C

Specification of the RhoVeR System

This appendix describes the Virtual Reality system as designed by the members of the Rhodes Virtual Reality Special Interest Group. The system consists of a number of processing modules capable of running on a variety of platforms and contains the communication modules to allow transfer of data between these various architectures.

This specification details the function of each module and the manner in which interaction between the modules is expected to occur.

C.1 Overview

Each virtual world will contain a number of instances of various types of modules. Each module consists of some data associated with a process. Each process is capable of running concurrently with any other process.

The processes communicate using two mechanisms. An event-passing facility allows any process to communicate with any other process. A virtual shared memory makes a common data structure available to all processes.

C.2 Interprocess Communication Facilities

C.2.1 Event-passing

All processes are capable of communicating directly with any other process by sending it a message (referred to in this document as an event). The possible events are predefined. Most processes will contain an event processing loop which will determine their behaviour when an event of a certain type is received.

C.2.2 The virtual shared memory

The virtual shared memory maintains a data structure which is replicated on all machines used by the virtual reality system. Only one copy of this replicated database will be maintained per machine, regardless of the number of modules running on that machine. Any process may read from this data structure. The data structure contains an entry for every object process (defined later), and only the corresponding object process, or its parent (defined later), may update that entry. Updates are achieved by sending an update event to the VSM Manager module on the machine.

C.3 The global data structures

C.3.1 The distributed data base

The data base distributed by the VSM consists of a table containing entries for every module in the virtual world. Each record in the table consists of the following fields:

- Identifier : This is a unique value for each module in the world.)
- Type of module : Allows object modules to be distinguished so that the relevance of the other fields can be determined.
- Position : Position of the object in the virtual world.
- Orientation : Orientation of the object in the virtual world.
- Boundary : Border of the object, for collision detection. At present this will be the radius of the bounding sphere.
- Parent identifier : Identifier of the parent object, equal to its own Identifier if it has no parent.
- Controller identifier: Identifier of the controlling object.

- Set of change counters : Give the number of updates to the shape data below to allow processes to update local copies when these change.
- Generic attributes : attributes which may be useful in various worlds. A fixed number are available and will be specified as a table containing pairs of values, the attribute identifier (e.g. Mass, Density) and the attribute value (e.g. 10kg, $5g/m^3$).

C.3.2 The shape data

Each object process contains some large tables of data that may be used by other objects. These tables are not used sufficiently often to justify distributing them everywhere. They will be sent in response to events requesting them, usually when the requesting process notices a change in the change counter for the table.

The following tables may be found:

- Polygon data : The vertex information for the shape of the object
- Colour : Colour values for the pieces of the object
- Texture : Details of texture maps for pieces of the object
- Generic tables : For temperature and other characteristics of the object
- Device data table : Raw device data for when the object is associated with a particular device
- World attribute list : A list of attributes active in a particular world, usually maintained by the world module.
- Machine name table : A list of address for all other modules, indexed by the identifier field of the distributed data base, usually maintained by the world module.

C.3.3 Local values

Each object will contain a tree of its child objects. This will not be shared.

C.4 The modules

The following modules are available. Each module description gives the function of the module and specifies the manner in which it must respond to events.

All modules share a common event response structure. They will contain the following skeleton:

```
Loop
    Event = GetEvent ();
    Case Event of
        —
        —
        —
    EndCase
EndLoop
```

Some modules, for example the input device drivers which do not respond to incoming events, can be exempted from the event polling and evaluation.

At startup, each module must send an event to the world module specifying its address.

C.4.1 The communication modules

C.4.1.1 The Virtual Shared Memory Manager module

The VSM Manager module has one instance per machine. It accepts only update events and discards those which are from processes that do not have appropriate permission to update the data base. It is responsible for transmitting the updates to other machines involved in the virtual world system.

The VSM manager responds to two events, an Update from a process wishing to modify its own data, and an UndergroundUpdate from other VSM managers to transfer approved updates from other machines. The response to these events is as follows:

```
Update :
    Check if sending process owns the field to be updated
    If not, return immediately, no error message is sent
    Update local entry
    Send UndergroundUpdates to the other VSM Managers

UndergroundUpdate :
    Update local entry
```

The VSM Manager has a rôle to play at system startup. The world module starts up one VSM Manager per machine. The VSM Manager must start any other modules local to that machine.

C.4.2 The World Control modules

C.4.2.1 The World module

The world module provides centralised control and decides policy for each world. Different worlds will be completely independent systems whose interaction will be through the corresponding world control modules.

The world modules provides attribute control for the other modules, to regulate a consistent world view. An attribute list may be retrieved from the world module to set the default behaviour of the object modules.

The world module may also have a role to play in centralised object control, and in access control to the world. It can also enforce global attributes, such as gravity and collision detection.

The world module maintains a table of addresses for each module in the world. This table is part of the shape data for the world module.

The world module is involved in system initialization. It is started first and is responsible for starting VSM Managers on each machine involved in the system. As modules are started up, they report their addresses to the world module, which must then update its table.

C.4.2.2 The Object modules

The object modules control objects in the virtual world. Each object is supplied with a standard event-handling routine which controls the manner in which it responds to incoming events. Only if this routine permits will the object call a user specified routine to react to the event. In some cases both the user routine and the default routine will execute.

Objects may be grouped in hierarchies. This hierarchy is a tree structure with the root node referred to as the parent object. Unless an event is specifically intended for the child process, it will be directed to the parent object. The parent will then send any relevant information to its children.

Objects are also responsible for maintaining and distributing their shape data on request. This is normally handled by the default event processing routines.

C.4.3 Output Modules

C.4.3.1 Video Output

This renders the world from the viewpoint of a particular object. It may have to query object shape databases for information needed to draw the object. These queries will only occur if the change counters have changed in value.

C.4.4 Input Modules

C.4.4.1 Device drivers

These interact with the input devices and transmit their raw data to the object representing the device. For example, finger positions are transmitted to the hand object.

C.5 Event-passing

Event-passing is handled at a lower level than the sections described previously. The interface to the event handling routines is handled by two routines:

- Send Event: sends an event of a particular type, together with any required data, to a specified process.
- Get Event: if an event is available, then the type of event, source process and any additional data is returned, otherwise NULL is returned. The data will be in the correct form for the architecture; any conversion necessary is performed by the Get Event procedure.

The data component of the event and its data is converted to a standard format (currently that used by Sparc Solaris 2.2) as part of SendEvent, and converted back to a format suitable for the local processor as part of GetEvent. Currently this is done on a global basis by exchanging the endian order on groups of 4 bytes.

C.5.1 Send Event

The send event routine will operate as follows:

void SendEvent (Destination, EventType, EventDataSize, EventData)

1. If there is no existing connection with the destination process:
    (a) Fetch the destination address from the world module.
    (b) Open a connection to the destination process.
2. Add the event to the queue of outgoing messages.
3. Attempt to send messages from the queue.
4. Poll incoming connections for events, and add any to the incoming queue.

C.5.2 Get Event and GetMatchingEvent

The GetEvent routine will operate as follows:

1. Check for, and open any new connections to other processes.
2. Poll incoming connections for events, and add any to the incoming queue.
3. Attempt to send messages from the outgoing queue.
4. If there is an event in the incoming queue which matches the required criteria, then return that event.
5. Return NULL.

GetMatchingEvent is intended to allow events to be received out of order, in the special cases where a reply is required before any further processing can be done. GetEvent uses the same function, but will match the first available event.

The format conversion occurs just before the events are added to the appropriate queues.

Bibliography

[Bangay 1993] Bangay S. (1993) *Parallel Implementation of a Virtual Reality System on a Transputer Architecture.* Masters Thesis, Technical Document PPG 93/10, Rhodes University.

[Barr 1984] Barr A. (1984) *Global and Local Deformations of Solid Primitives.* Computer Graphics (Proceedings of SIGGRAPH '84), 18(3), pp. 21-30.

[Bartels *et al 1987]* Bartels R., Beatty J. and Barsky B. (1987) *An Introduction to Splines for use in Computer Graphics and Geometric Modelling.* Morgan Kaufmann.

[Bill and Lodha 1994] Bill J. and Lodha S. (1994) *Computer Sculpting of Polygonal Models using Virtual Tools.* Technical Report UCSC-CRL-94-27, University of California, Santa Cruz.

[Borrel and Bechmann 1992] Borrel P. and Bechmann D. (1991) *Deformation of N-dimensional Objects.* International Journal of Computational Geometry and Applications, 1(4), pp. 427-453

[Brijs *et al* 1993] Brijs P., Hoek, T., Van der Mast C. and Smets G. *Designing in Virtual Reality: Modelling Objects in a Virtual Environment (MOVE).* Technical Report 93-91, Delft University of Technology.

[Burden and Faires 1993] Burden R. and Faires J. (1993) *Numerical Analysis* [5th ed]. PWS Publishing Company, Boston.

[Butterworth *et al* 1992] Butterworth J., Davidson A., Hench S. and Olano T. (1992) *3DM: A Three Dimensional Modeler Using a Head-Mounted Display.* Proceedings of 1992 Symposium on Interactive 3D Graphics, ACM SIGGRAPH, pp. 135-138.

[Celniker and Gossard 1991] Celniker G. and Gossard D. (1991) *Deformable Curve and Surface Finite Elements for Free-Form Shape Design.* Computer Graphics (Proceedings of SIGGRAPH '91), 25(4), pp. 257-266.

[Chadwick *et al* 1989] Chadwick J., Haumann D. and Parent R. (1989) *Layered Construction for Deformable Animated Characters.* Computer Graphics (Proceedings of SIGGRAPH '89), 23(3), pp. 243-252.

[Chapin *et al* 1994] Chapin W., Lacey T. and Leifer L. (1994) *DesignSpace: A Manual Interaction Environment for Computer Aided Design.* Proceedings of CHI '94, pp. 24-28.

[Coquillart 1987] Coquillart S. (1987) *A Control-Point-Based Sweeping Technique.* IEEE Computer Graphics and Applications, 7(11), pp. 36-45.

[Coquillart 1990] Coquillart S. (1990) *Extended Free-Form Deformation: A Sculpturing Tool for 3D Geometric Modeling.* Computer Graphics (Proceedings of SIGGRAPH '90), 24(4), pp. 187-196.

[Coquillart and Jancène 1991] Coquillart S. and Jancène P. (1991) *Animated Free-Form Deformation: An Interactive Animation Technique.* Computer Graphics (Proceedings of SIGGRAPH '91), 25(4), pp. 23-26.

[Foley *et al 1991]* Foley J., Van Dam A., Feiner S. and Hughes J. (1991) *Computer Graphics: Principles and Practice* [2nd ed]. Addison-Wesley Publishing Company.

[Galyean and Hughes 1991] Galyean T. and Hughes J. (1991) *Sculpting: An Interactive Volumetric Modeling Technique.* Computer Graphics (Proceedings of SIGGRAPH '92), 25(4), pp. 267-274.

[Golub and Van Loan 1989] Golub G. and Van Loan C. (1989) *Matrix Computations* [2nd ed]. Johns Hopkins University Press.

[Gourret *et al* 1989] Gourret J., Magnenat-Thalmann N. and Thalmann D. (1989) *Simulation of Object and Human Skin Deformation in a Grasping Task.* Computer Graphics (Proceedings of SIGGRAPH '89), 23(3), pp. 21-30.

[Greville 1960] Greville T. (1960) *Some Applications of the Pseudoinverse of a Matrix.* SIAM Review, 2(1), pp. 15-22.

[Hoppe *et al* 1992] Hoppe H., DeRose T., Duchamp T., McDonald J. and Stuetzle W. *Surface Reconstruction from Unorganized Points.* Computer Graphics (Proceedings of SIGGRAPH '92), 26(2), pp. 71-78.

[Hsu *et al* 1992] Hsu W., Hughes J. and Kaufman H. (1992) *Direct Manipulation of Free-Form Deformations.* Computer Graphics (Proceedings of SIGGRAPH '92), 26(2), pp. 177-182.

[Jacobson 1994] Jacobson R. (1994) *Virtual Worlds: A New Type of Design Environment.* Virtual Reality World, 2(3), pp. 46-52.

[Johnson *et al* 1993] Johnson L., Riess R. and Arnold J. (1993) *Introduction to Linear Algebra* [3rd ed]. Addison-Wesley Publishing Company.

[Latta 1991] Latta J. (1991) *When Will Reality Meet the Marketplace?* Proceedings of Virtual Reality '91, Meckler Publishing, pp. 109-141.

[Lamousin and Waggenspack 1994] Lamousin H. and Waggenspack W. (1994) *NURBS-Based Free-Form Deformation* IEEE Computer Graphics and Applications, 14(6) pp. 59-65.

[Lawson and Hanson 1974] Lawson C. and Hanson R. (1974) *Solving Least Squares Problems.* Prentice-Hall, Englewood Cliffs, NJ.

[Metaxas and Terzopoulos 1992] Metaxas D. and Terzopoulos D. (1992) *Dynamic Deformation of Solid Primitives with Constraints.* Computer Graphics (Proceedings of SIGGRAPH '92), 26(2), pp. 309-312.

[Miller 1986] Miller J. (1986) *Sculptured Surfaces in Solid Models: Issues and Alternative Approaches.* IEEE Computer Graphics and Applications, 6(12), pp. 37-48.

[Nielson 1993] Nielson G. (1993) *CAGD's Top Ten: What to Watch.* IEEE Computer Graphics and Applications, 13(1), pp. 35-37.

[Noble 1969] Noble B. (1969) *Applied Linear Algebra.* Prentice-Hall, Englewood Cliffs, NJ.

[Qin and Terzopoulos 1995] Qin H. and Terzopoulos D. (1995) *Dynamic Manipulation of Triangular B-Splines.* Proceedings of the Third Symposium on Solid Modeling and Applications, ACM Press, pp. 351-360.

[Requicha and Rossignac 1992] Requicha A. and Rossignac J. *Solid Modeling and Beyond.* IEEE Computer Graphics and Applications, 12(5), pp. 34-44.

[Rheingold 1991] Rheingold H. (1991) *Virtual Reality.* Summit Books.

[Sachs *et al* 1991] Sachs E., Roberts A. and Stoops D. (1991) *3-Draw: A Tool for Designing 3D Shapes.* IEEE Computer Graphics and Applications, 11(6), pp. 18-26.

[Schroeder *et al* 1992] Schroeder W., Zarge J. and Lorensen W. (1992) *Decimation of Triangle Meshes.* Computer Graphics (Proceedings of SIGGRAPH '92), 26(2), pp. 65-70.

[Schumaker 1993] Schumaker L. (1993) *Triangulations in CAGD.* IEEE Computer Graphics and Applications, 13(1), pp. 47-52.

[Sederberg and Parry 1986] Sederberg T. and Parry S. (1986) *Free-Form Deformation of Solid Geometric Models.* Computer Graphics (Proceedings of SIGGRAPH '86), 20(4), pp. 151-160.

[Shaw and Green 1994] Shaw C. and Green M. (1994) *Two-Handed Polygonal Surface Design.* Proceedings of UIST '94, pp. 205-212, ACM SIGGRAPH/SIGCHI.

[Shimada and Gossard 1995] Shimada K. and Gossard D. (1995) *Bubble Mesh: Automated Triangular Meshing of Non-Manifold Geometry by Sphere Packing.* Proceedings of the Third Symposium on Solid Modeling and Applications, ACM Press, May, pp. 409-419.

[Stoer and Bulirsch 1983] Stoer J. and Bulirsch R. (1983) *Introduction to Numerical Analysis.* Springer-Verlag, New York.

[Terzopoulos and Fleischer 1988] Terzopoulos D. and Fleischer K. (1988) *Modeling Inelastic Deformation: Viscoelasticity, Plasticity, Fracture.* Computer Graphics (Proceedings of SIGGRAPH '88), 22(4), pp. 269-278.

[Welch and Witkins 1992] Welch W. and Witkins A. (1992) *Variational Surface Modeling.* Computer Graphics (Proceedings of SIGGRAPH '92), 26(2), pp. 157-165.

[Welch and Witkins 1994] Welch W. and Witkins A. (1994) *Free-Form Shape Design using Triangulated Surfaces.* Computer Graphics (Proceedings of SIGGRAPH '94), pp. 247-256.

[Wördenweber 1983] Wördenweber B. (1983) *Surface Triangulation for Picture Production.* IEEE Computer Graphics and Applications, 3(8), pp. 45-51.